Article

Sexual arousal gates visual processing during *Drosophila* courtship

https://doi.org/10.1038/s41586-021-03714-w

Received: 4 September 2020

Accepted: 9 June 2021

Published online: 7 July 2021

Check for updates

Tom Hindmarsh Sten[1], Rufei Li[1], Adriane Otopalik[1] & Vanessa Ruta[1]✉

Long-lasting internal arousal states motivate and pattern ongoing behaviour, enabling the temporary emergence of innate behavioural programs that serve the needs of an animal, such as fighting, feeding, and mating. However, how internal states shape sensory processing or behaviour remains unclear. In *Drosophila*, male flies perform a lengthy and elaborate courtship ritual that is triggered by the activation of sexually dimorphic P1 neurons[1–5], during which they faithfully follow and sing to a female[6,7]. Here, by recording from males as they court a virtual 'female', we gain insight into how the salience of visual cues is transformed by a male's internal arousal state to give rise to persistent courtship pursuit. The gain of LC10a visual projection neurons is selectively increased during courtship, enhancing their sensitivity to moving targets. A concise network model indicates that visual signalling through the LC10a circuit, once amplified by P1-mediated arousal, almost fully specifies a male's tracking of a female. Furthermore, P1 neuron activity correlates with ongoing fluctuations in the intensity of a male's pursuit to continuously tune the gain of the LC10a pathway. Together, these results reveal how a male's internal state can dynamically modulate the propagation of visual signals through a high-fidelity visuomotor circuit to guide his moment-to-moment performance of courtship.

In *Drosophila*, mate recognition triggers a striking switch in a male's behaviour, as he transitions from being apathetic or 'blind' to a female to vigorously chasing and singing to her to entice her to copulate[6,7]. Recent work has identified a small population of sexually dimorphic P1 neurons as a central node in the courtship circuitry that are tuned to the pheromones of conspecific female mates[8–12] and regulate a male's entry into courtship[1–5]. Indeed, transient activation of P1 neurons drives persistent courtship displays even towards inanimate objects, suggesting that these neurons gate an enduring state of sexual arousal[5,8,10,13–15]. We sought to investigate how this internal state restructures sensorimotor circuits to convert a female from an indifferent visual object to a target of desire.

Courtship reflects a dynamic arousal state

To explore how sensory processing is altered by a male's arousal, we developed a virtual-reality visual system based on previous hardware designs (Weisman, J. L. & Maimon, G., personal communication; Fig. 1a, Extended Data Fig. 1) in which a tethered male can court a 'female' represented as a high-contrast dot projected onto a conical screen. Optogenetic activation of P1 neurons expressing CsChrimson induced male flies to chase the autonomously moving visual target for several metres in this 2D virtual world while performing the ipsilateral wing extensions that are characteristic of the courtship song (Fig. 1b, Extended Data Fig. 2a, b, Supplementary Video 1). Males maintained the target at close range within the centre of their visual field during P1 activation, replicating the oriented pursuit exhibited in free courtship, whereas wild-type males showed no behavioural response to the visual stimulus (Fig. 1c, Extended Data Fig. 2b–g, Supplementary Video 2).

The dynamics of a male's arousal have been difficult to study during natural social encounters, where continuous sensory feedback from another fly could contribute to its regulation. To dissociate changes in a male's external sensory environment from his internal state we monitored his response to a dot that traversed back and forth along an arc at a constant angular velocity. Tethered males were initially indifferent to this visual stimulus but after brief (3-s) optogenetic activation of P1 neurons they began to track it for many minutes while performing unilateral wing extensions (Fig. 1d–f, Supplementary Video 3), consistent with evidence that P1 neurons trigger enduring courtship pursuit[5,10,13–15] (Extended Data Fig. 4o). The vigour of other visually guided behaviours, such as optomotor turning in response to wide-field motion[16], was not enhanced (Extended Data Fig. 4g–i), highlighting the specificity of P1-evoked arousal.

To quantify how the intensity of a male's courtship unfolded over time, we defined a 'tracking index' that reflects both the fidelity and vigour of his visual pursuit (see Methods; Fig. 1f, Extended Data Fig. 3a–d). Aroused males did not incessantly court the visual target. Rather, the intensity of their pursuit fluctuated during a trial. Occasionally, they even temporarily disengaged and ceased tracking despite the continued presence of the visual stimulus (Fig. 1e, f, Extended Data Fig. 3b, g). Disengaged males were indistinguishable from unaroused animals on the basis of their behavioural kinematics but remained primed to rapidly reinitiate courtship (Extended Data Fig. 3h–k). Moreover, males that were induced to disengage by briefly removing the visual stimulus (for 30 s) quickly resumed pursuit when it was reintroduced (Extended Data Fig. 4a, b), demonstrating that their arousal state remained latent even in the absence of continuous sensory input or behaviour. Over

[1]Laboratory of Neurophysiology and Behavior, The Rockefeller University, New York, NY, USA. ✉e-mail: ruta@rockefeller.edu

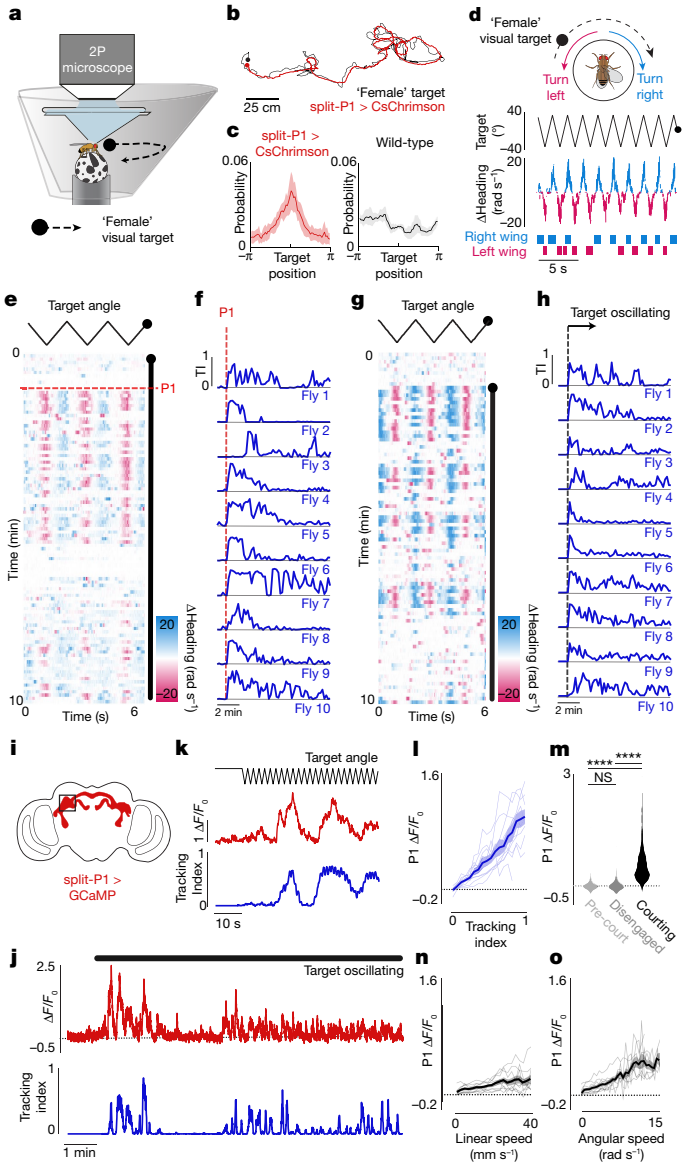

Fig. 1 | P1 neurons release and reflect a dynamic state of sexual arousal. **a**, Schematic of behavioural setup. **b**, Two-dimensional path of a male courting a pseudo-randomly moving target in closed-loop. **c**, Angular position of the target relative to males expressing CsChrimson in P1 neurons or wild-type males during tethered closed-loop courtship. **d**, Example of a courting male displaying turning (middle) and wing extensions (bottom) to the visual target in open-loop. **e**, Example of a male's turning throughout a courtship trial. Each row consists of three stimulus cycles, with the target angle shown at the top. Red line indicates 3-s P1 activation; black bar indicates when the visual stimulus is oscillating. **f**, Tracking index (TI; see Methods) for ten flies following optogenetic activation of P1 neurons. Top trace is the same animal as in **e**. **g**, **h**, Same as **e**, **f** but for spontaneously initiated courtship trials. **i**, Schematic of P1 neurons (red) expressing GCaMP in the brain of a male fly with black box denoting approximate imaging region of interest (ROI). **j**, Example of P1 neuron activity ($\Delta F/F_0$) and tracking index of a male during a courtship trial. **k**, Zoomed-in view of the onset of courtship in **j**. **l**, Activity of P1 neurons (average $\Delta F/F_0$) plotted against tracking index. **m**, Distribution of P1 activity ($\Delta F/F_0$) before courtship was initiated (pre-court), during periods when males were temporarily disengaged, and during active courtship pursuit (courting; tracking index > 0.3). **n**, **o**, Activity of P1 neurons (average $\Delta F/F_0$) plotted against the male's linear speed (**n**) or angular velocity (**o**). Shaded lines show mean ± s.e.m.; thin lines denote individual animals; NS, $P > 0.05$; ****$P < 0.0001$. Details of statistical analyses and sample sizes are given in Supplementary Table 1.

time, the probability of a male transitioning from disengagement to active pursuit decreased, indicating that his arousal slowly waned (Extended Data Figs. 3j, k, 4o).

Persistent courtship of the virtual target could also be triggered by allowing males to sample the pheromones on a conspecific female, replicating his assessment of a prospective mate[6,10–12] (Extended Data Fig. 4c–f). However, although pheromone pathways converge onto P1 neurons[10,11], these chemical cues are not essential to arouse a male[17,18]. Indeed, by modifying the stimulus to more closely mimic the natural statistics of female motion (Extended Data Fig. 4j–l, Supplementary Video 4) and socially isolating males to enhance their mating drive[8,14,17,19], we found that males would spontaneously initiate courtship even in the absence of exogeneous activation of P1 neurons (Fig. 1g, h, Extended Data Fig. 4m–o, Supplementary Video 5). Visual cues are therefore sufficient to release a persistent state of arousal in *Drosophila* males.

P1 activity reflects pursuit intensity

To examine the dynamics of P1 neurons during spontaneous courtship, we performed functional calcium imaging of their axonal terminals using a selective genetic driver line[15] (Fig. 1i). P1 neurons were robustly activated as males initiated courtship, even when they began tracking many seconds after presentation of the visual stimulus (Fig. 1j, k, Extended Data Fig. 5d). Following courtship onset, P1 activity continued to fluctuate throughout the duration of a courtship bout, providing an ongoing representation of the intensity of a male's pursuit and giving rise to a tight correlation with a male's tracking index over the course of a trial (Fig. 1j–l, $r = 0.69 \pm 0.075$ (mean ± s.d.), Extended Data Figs. 5b, 6f, j). P1 activity was disproportionally higher at the initiation of courtship (Extended Data Fig. 5c–g), indicating that these neurons may signal additional aspects of a male's internal state or behaviour that we are not measuring.

P1 activity was poorly correlated with the visual stimulus ($r = -0.10 \pm 0.008$), but displayed a weak relationship to a male's linear ($r = 0.23 \pm 0.099$) and angular speed ($r = 0.28 \pm 0.062$; Fig. 1n, o, Extended Data Figs. 5a, 6f–j)—probably because males must run and turn to track the target. Indeed, P1 fluorescence remained low in sexually unaroused males turning vigorously in response to wide field motion, confirming that P1 activity more closely aligns with a male's courtship state than the kinematics of his pursuit (Extended Data Fig. 6a–e, k–o). Moreover, although the activity of P1 neurons was time-locked to the initiation of courtship, their calcium signals decayed back to baseline when males transiently ceased courting, indicating that a male's enduring arousal is stored either subcellularly or in the activity patterns of downstream neurons (Fig. 1j, k, m). Therefore, while P1 neurons gate entry into a lasting arousal state[10,13–15], their ongoing activity corresponds to the moment-to-moment changes in the intensity of a male's courtship pursuit.

LC10a gain is modulated during courtship

LC10a visual projection neurons have been identified as motion detectors that convey retinotopically organized visual signals to the anterior optic tubercle (AOTu)[20–22], and are essential for accurate tracking of conspecifics during courtship[20]. Consistent with this role, unilateral optogenetic silencing of LC10a neurons strongly attenuated turning towards the ipsilateral visual target during tethered courtship (Extended Data Fig. 7a–c). Monitoring of GCaMP activity in the LC10a axon terminals in the AOTu of unaroused males revealed only weak responses to the fictive 'female'. At the initiation of courtship pursuit, however, LC10a axon terminals became robustly activated each time the visual target swept across the male's ipsilateral hemifield (Fig. 2a, b, d, Extended Data Fig. 7d–h). The shape of LC10a responses remained unchanged, pointing to alterations in their gain rather than changes to their tuning (Fig. 2e). Notably, during periods when males transiently

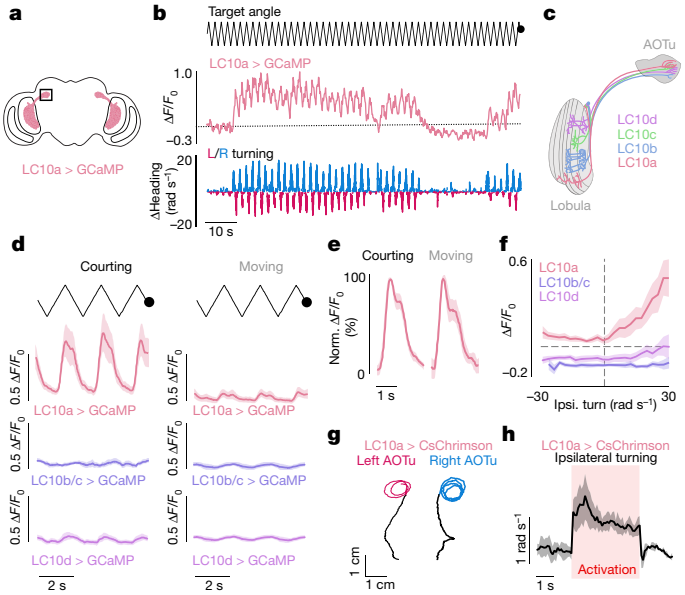

Fig. 2 | Modulation of LC10a neurons during courtship. a, Schematic of LC10a neurons expressing GCaMP with black box denoting approximate imaging ROI. **b**, Example of LC10a responses during a courtship trial. Top, angular position of the target; middle, activity ($\Delta F/F_0$) of LC10a neurons; bottom, angular velocity of male. **c**, Schematic of subtypes of LC10 neurons that innervate the AOTu. **d**, Responses of LC10a, LC10b/c, and LC10d neurons (average $\Delta F/F_0$) to the visual target during periods of courtship (left) or general locomotion (right). **e**, Responses of LC10a neurons (average $\Delta F/F_0$ normalized to peak activity) during courtship and general locomotion. **f**, Activity (average $\Delta F/F_0$) of LC10a, LC10b/c, and LC10d neurons plotted against male ipsiversive (ipsi.) turning velocity. **g**, Sample 2D paths of two males before (black) and during optogenetic activation of LC10a neurons in the left (red) or right (blue) hemisphere. **h**, Average evoked ipsilateral turning during unilateral stimulation of LC10a neurons expressing CsChrimson. Shaded lines show mean ± s.e.m.; details of statistical analyses and sample sizes are given in Supplementary Table 1.

ceased tracking, LC10a neurons returned to their low baseline activity level (Fig. 2b, Extended Data Fig. 7e), highlighting that the gain of these pathways is modulated on a moment-to-moment timescale.

Although males increased their velocity during courtship, the gain of LC10a neurons was significantly more correlated with a male's tracking index ($r^2 = 0.63 \pm 0.16$) than either his linear ($r^2 = 0.29 \pm 0.26$) or angular speed ($r^2 = 0.43 \pm 0.21$; Extended Data Fig. 8a–f). To further dissociate the gain of LC10a neurons from the motor implementation of visual pursuit, we took advantage of the fact that males cannot turn left and right simultaneously and introduced a second target to courting males whose position was opposite to the first, so that both eyes received identical stimulation (Extended Data Fig. 8g). LC10a neurons continued to respond even when males failed to turn towards a visual stimulus or turned in the contralateral direction (Extended Data Fig. 8g–i), thus decoupling the gain enhancement of LC10a neurons from the kinematics of tracking (Extended Data Fig. 8i, j).

To investigate the specificity of the LC10a gain modulation, we examined the responses of LC10b, LC10c, and LC10d visual projection neurons—which are morphologically similar to LC10a and sample from overlapping layers of the lobula[21,22] (Fig. 2c)—but found that their responses to the target remained unchanged as males initiated courtship (Fig. 2d, Extended Data Fig. 8k, l). Consequently, only LC10a neurons displayed a tight correspondence between the magnitude of evoked visual responses and a male's ipsilateral turns (Fig. 2f). Supporting this specificity, the female connectome[23] indicates that LC10a–d neurons display distinct patterns of synaptic connectivity within the AOTu (Extended Data Fig. 9a–f), which suggests that they potentially comprise parallel visual streams that can be independently modulated.

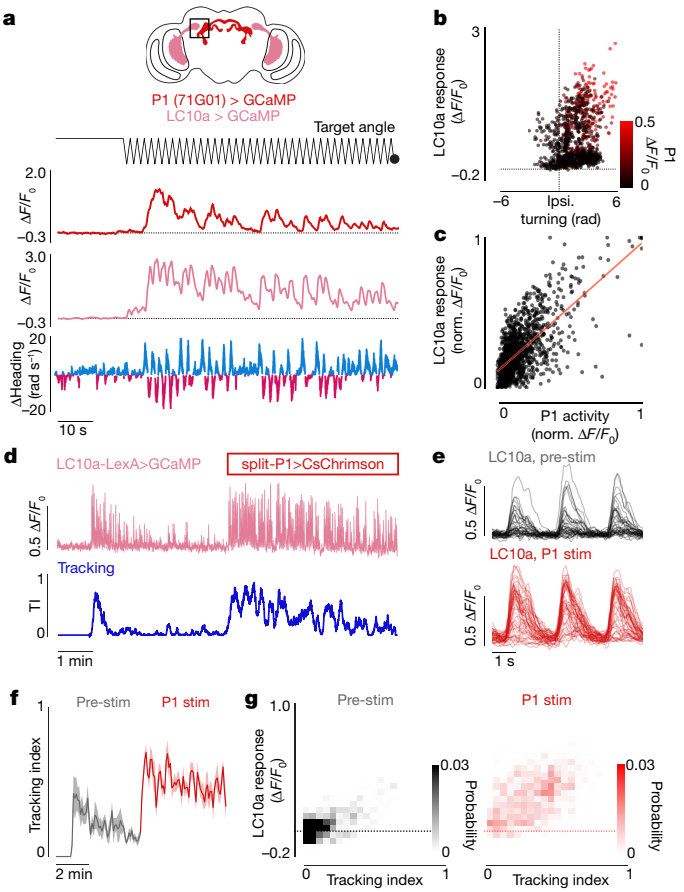

Fig. 3 | P1 neurons represent intensity of courtship and acutely regulate pursuit. a, Top, schematic of LC10a and P1 neuron morphology, both expressing GCaMP. Plots below, from top to bottom rows: angular position of the target; functional responses ($\Delta F/F_0$) of P1 neurons; functional responses ($\Delta F/F_0$) of LC10a; and angular velocity of male. **b**, LC10a activity ($\Delta F/F_0$) evoked by a single stimulus sweep plotted against the male ipsiversive turning response, colour coded by the average P1 activity in the same time period. **c**, Normalized LC10a responses to each stimulus sweep plotted against normalized average P1 activity in the same time period ($r = 0.68$, $P < 0.00001$, $m = 0.85$, $b = 0.10$). **d**, Example of tracking index and the activity of LC10a neurons in a male before and during optogenetic activation of P1 neurons expressing CsChrimson. **e**, Responses ($\Delta F/F_0$) of LC10a neurons during spontaneous courtship (top, pre-stim) and P1 activation (bottom, P1 stim) for the male in **d**. **f**, Average tracking index across animals over trials structured as in **d**. **g**, Density plots of tracking index against activity ($\Delta F/F_0$) of LC10a neurons on each stimulus cycle before (left) and during P1 activation (right) across males. Shaded line plots are mean ± s.e.m. Details of statistical analyses and sample sizes are given in Supplementary Table 1.

Consistent with previous work[20,21], unilateral optogenetic activation of LC10a axon terminals drove acute ipsilateral turning (Fig. 2g, h), which indicates that LC10a neurons may underlie a male's faithful pursuit. Indeed, anterograde tracing using trans-Tango[24] in males and the female connectome[23] revealed that the downstream synaptic partners of LC10a neurons richly innervate the lateral accessory lobe (LAL; Extended Data Fig. 9g–k), a neuropil that is targeted by multiple descending neurons that have been implicated in the control of steering behaviour[25–27]. Sexual arousal is thus poised to gate the flow of sensory signals through a concise visuomotor circuit.

P1 neurons regulate LC10a signalling

Although P1 neurons do not directly innervate the AOTu, the tight correspondence between P1 activity and ongoing changes in the intensity

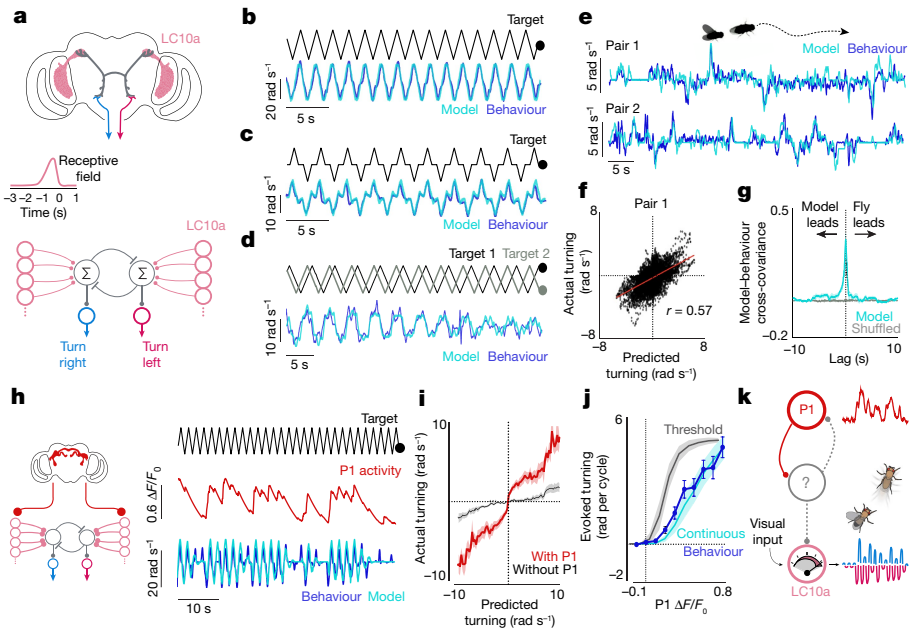

Fig. 4 | A network model of LC10a neurons recapitulates male pursuit. **a**, Top, proposed anatomy of the LC10a circuit with LAL neurons (grey) and descending neurons (blue/red); middle, LC10a temporal receptive fields; bottom, network model. **b**–**d**, Predicted versus actual turning of aroused males to a single target (**b**), a single target that pauses for 500 ms in front of the male (**c**), and two targets oscillating at different frequencies (**d**). **e**, Examples of predicted and actual turning of males during free courtship. **f**, Predicted versus actual turning velocity across a free courtship trial (pair 1; $r = 0.56$). **g**, Average normalized cross-covariance between predicted and actual turning during free courtship and shuffled controls. **h**, Left, schematic of network model incorporating P1 activity; right, example of actual versus predicted turning when P1 activity (red) is included in model. **i**, Actual versus predicted turning of courting males for models with and without P1 activity. **j**, Total ipsiversive turning in response to a stimulus sweep plotted against P1 activity ($\Delta F/F_0$), as predicted by a continuous or threshold model. Blue, average behavioural data. **k**, Schematic of the segregated circuit in which P1 activity regulates LC10a gain. Shaded lines show mean ± s.e.m.; details of statistical analyses and sample sizes are given in Supplementary Table 1.

of a male's courtship pursuit (Fig. 1i–l) suggests that they may signal to LC10a neurons to regulate their gain. Consistent with this possibility, synchronous recordings demonstrated that the activity of P1 and LC10a neurons was highly correlated (Fig. 3a, Extended Data Fig. 10a), and jointly reflected a male's ipsilateral turning (Fig. 3b). Indeed, the magnitude of P1 activity was near linearly ($m = 0.86$) predictive of the amplitude of LC10a responses evoked by the visual target ($r = 0.68$, $P < 0.00001$; Fig. 3c). Moreover, exogenous activation of P1 neurons drove LC10a neurons to robustly respond to every sweep of the visual stimulus, transforming the idiosyncratic structure of spontaneous courtship to incessant high-fidelity tracking (Fig. 3d–g).

P1 modulation could gate the flow of all visual signals through the LC10a pathway, or could reshape the receptive fields of LC10a neurons to preferentially enhance responses to the visual profile of a female. However, the responses of LC10a neurons to a panel of diverse visual targets—including moving dots of various angular sizes, long bars, or a slowly expanding sphere—were uniformly amplified by P1 activation (Extended Data Fig. 10b–h). State-dependent modifications to visual processing therefore appear to reflect alterations in the gain of LC10a neurons rather than a restructuring of their receptive fields, suggesting either that LC10a neurons serve as the direct target of modulation or that their input pathways are uniformly amplified.

Notably, LC10a responses to all visual stimuli were in aggregate stronger to progressive than regressive motion in both unaroused and courting males (Extended Data Fig. 10b–e, i). The elevated signalling in aroused males made the direction selectivity of LC10a neurons appear more pronounced (Extended Data Fig. 10b–e), however, potentially explaining why these neurons were previously characterized as relatively insensitive to the direction of visual motion[20]. Examining correlated pixels within the AOTu, which are likely to correspond to individual LC10a axonal boutons (Extended Data Fig. 11a), confirmed that direction selectivity is a general characteristic of this population (Extended Data Fig. 11b–d). The behavioural responses of courting males mirrored this directional tuning, as they executed ipsiversive turns only when the stimulus swept progressively, but not regressively, in front of one eye (Extended Data Fig. 11e).

A network model of courtship pursuit

To test whether P1-mediated modulation of LC10a signalling could capture the dynamics of courtship pursuit, we constructed a network model to mimic the concise architecture of this visuomotor circuit. We modelled LC10a neurons as a population of integrate-and-fire units, each of which covered a portion of the male's visual field, with 15° of binocular overlap[28], and used the motion-based receptive fields estimated by Ribeiro et al.[20] to structure excitatory input (Fig. 4a). Activity in the left and right LC10a populations was integrated by downstream units, which triggered ipsilateral turns whose magnitude was proportional to the difference in firing rate between them.

Small deviations in the model's temporal receptive field strongly degraded its performance, indicating that the measured tuning properties of LC10a neurons are well-suited to replicate a male's pursuit (Fig. 4b, Extended Data Fig. 11g). Moreover, consistent with our functional and behavioural analyses, complete selectivity to progressive motion was necessary for the model to accurately track a simple visual target in a time-locked fashion (Extended Data Fig. 11f). The model also correctly predicted that this direction selectivity, coupled with the small region of binocular overlap, enables males to anticipate the future position of the 'female' target when it briefly stops at the centre of his field of view (Fig. 4c, $r = 0.86$, $P < 0.00001$; Extended Data Fig. 11h), giving rise to an overshoot in the male's turning. This is consistent with behavioural evidence from houseflies that males may predict the motion of a target as it passes from one visual field to the next during courtship, enhancing the fidelity and continuity of pursuit[29].

To test whether the linear integration between LC10a signals in the two hemispheres could predict the direction and strength of a male's

turns, we introduced a second visual target that oscillated at 98% of the velocity of the first target, allowing us to measure a male's steering behaviour as the phase relationship between the two dots varied (Supplementary Video 6). Males presented with this complex stimulus responded nearly indistinguishably from our model; they stopped responding to visual motion when the targets were opposite in phase, and otherwise preferentially turned in response to the leading target (Fig. 4d, $r = 0.83$, $P < 0.00001$, Extended Data Fig. 11i, j).

Inspired by classic studies of the control systems employed by other Dipteran species during aerial pursuit[29,30], we tested whether our model could also replicate the dynamics of freely moving males in natural courtship. Using just the estimated position of the female on the male's retina, the model accurately predicted the steering behaviour of courting males over many minutes (Fig. 4e–g, Extended Data Fig. 12; $r = 0.52 \pm 0.06$, $n = 6$ pairs, $P < 0.00001$ for all flies). Furthermore, by assuming that model males match their linear speed to that of the female, we could simulate the high-fidelity tracking of a courting male within a circular arena (Supplementary Video 7). The properties of this simple visuomotor circuit are thus largely sufficient to account for a male's faithful tracking of a female, although additional visual pathways are also likely to be engaged for long-distance orientation.

Finally, we reasoned that incorporating the ongoing activity of P1 neurons into our model should enhance its predictive power by accounting for fluctuations in a male's arousal during spontaneous courtship. We found that simply scaling the net input current of LC10a neurons by the experimentally measured activity of P1 neurons ($\Delta F/F$, Fig. 4h) significantly improved the model's accuracy (Fig. 4h, i, Extended Data Fig. 13b–d). The model no longer responded incessantly to the visual stimulus, but instead accurately predicted the intermittent bout structure of spontaneously courting males (Extended Data Fig. 13a). Consistent with the linear relationship between evoked LC10a responses and P1 activity (Fig. 3c), modelling the input of P1 neurons as a continuous-gain function yielded a linear relationship between P1 activity and the magnitude of a male's ipsiversive turns that closely matched the experimental data, while a threshold-based model predicted a sigmoidal relationship (Fig. 4j). Our modelling results thus suggest that the intensity of a male's courtship drive operates along a continuum, allowing P1 neurons to continuously regulate the strength of signalling through visuomotor circuits to shape ongoing behaviour (Fig. 4k).

Discussion

In the wild, *Drosophila* meet and mate on fermenting fruits, where diverse species frequently congregate[31]. Consequently, a male must not only be persistent in his courtship to entice choosy females to copulate[32], but also remain sensitive to sensory feedback to prevent continued pursuit of inappropriate or unreceptive mates. Here, we reveal a segregated circuit logic that balances this need for persistence and flexibility to guide a male's moment-to-moment performance of the courtship ritual. We find that courtship pursuit is mediated by a highly reliable visuomotor circuit whose gain is modulated on a moment-to-moment timescale by P1 neuron activity, which functions like a rheostat to control the propagation of visual signals in a graded manner. Consequently, the LC10a pathway lies dormant in the brain unless P1 neurons are active, rendering males effectively blind to the visual profile of a female until she is recognized as a potential mate. As the site of convergence for both excitatory and inhibitory sensory cues emanating from other flies[8–12,33], P1 neurons offer a powerful nexus for such ongoing behavioural control. Indeed, as inhibitory pheromone pathways directly impinge onto P1 neurons[10–12], they could acutely reverse the gain of LC10 signalling to suppress futile pursuit of an inappropriate mate. The dynamic gating of sensorimotor circuits we describe thus offers a mechanism to hone the expression of behavioural programs, suggesting a circuit instantiation for how a fixed and reflexive motor pattern can be unleashed via an innate releasing mechanism from classic ethology[34].

Online content

Any methods, additional references, Nature Research reporting summaries, source data, extended data, supplementary information, acknowledgements, peer review information; details of author contributions and competing interests; and statements of data and code availability are available at https://doi.org/10.1038/s41586-021-03714-w.

1. Kimura, K., Hachiya, T., Koganezawa, M., Tazawa, T. & Yamamoto, D. Fruitless and doublesex coordinate to generate male-specific neurons that can initiate courtship. *Neuron* **59**, 759–769 (2008).
2. von Philipsborn, A. C. et al. Neuronal control of *Drosophila* courtship song. *Neuron* **69**, 509–522 (2011).
3. Yamamoto, D. & Koganezawa, M. Genes and circuits of courtship behaviour in *Drosophila* males. *Nat. Rev. Neurosci.* **14**, 681–692 (2013).
4. Yu, J. Y., Kanai, M. I., Demir, E., Jefferis, G. S. X. E. & Dickson, B. J. Cellular organization of the neural circuit that drives *Drosophila* courtship behavior. *Curr. Biol.* **20**, 1602–1614 (2010).
5. Pan, Y., Meissner, G. W. & Baker, B. S. Joint control of *Drosophila* male courtship behavior by motion cues and activation of male-specific P1 neurons. *Proc. Natl Acad. Sci. USA* **109**, 10065–10070 (2012).
6. Bastock, M. & Manning, A. The courtship of *Drosophila melanogaster*. *Behaviour* **8**, 85–111 (1955).
7. Spieth, H. T. Courtship behavior in *Drosophila*. *Annu. Rev. Entomol.* **19**, 385–405 (1974).
8. Kohatsu, S. & Yamamoto, D. Visually induced initiation of *Drosophila* innate courtship-like following pursuit is mediated by central excitatory state. *Nat. Commun.* **6**, 6457 (2015).
9. Seeholzer, L. F., Seppo, M., Stern, D. L. & Ruta, V. Evolution of a central neural circuit underlies *Drosophila* mate preferences. *Nature* **559**, 564–569 (2018).
10. Clowney, E. J., Iguchi, S., Bussell, J. J., Scheer, E. & Ruta, V. Multimodal chemosensory circuits controlling male courtship in *Drosophila*. *Neuron* **87**, 1036–1049 (2015).
11. Kallman, B. R., Kim, H. & Scott, K. Excitation and inhibition onto central courtship neurons biases *Drosophila* mate choice. *eLife* **4**, e11188 (2015).
12. Zhang, S. X., Miner, L. E., Boutros, C. L., Rogulja, D. & Crickmore, M. A. Motivation, perception, and chance converge to make a binary decision. *Neuron* **99**, 376–388.e6 (2018).
13. Bath, D. E. et al. FlyMAD: rapid thermogenetic control of neuronal activity in freely walking *Drosophila*. *Nat. Methods* **11**, 756–762 (2014).
14. Inagaki, H. K. et al. Optogenetic control of *Drosophila* using a red-shifted channelrhodopsin reveals experience-dependent influences on courtship. *Nat. Methods* **11**, 325–332 (2014).
15. Hoopfer, E. D., Jung, Y., Inagaki, H. K., Rubin, G. M. & Anderson, D. J. P1 interneurons promote a persistent internal state that enhances inter-male aggression in *Drosophila*. *eLife* **4**, e11346 (2015).
16. Götz, K. G. & Wenking, H. Visual control of locomotion in the walking fruitfly *Drosophila*. *J. Comp. Physiol.* **85**, 235–266 (1973).
17. Agrawal, S., Safarik, S. & Dickinson, M. The relative roles of vision and chemosensation in mate recognition of *Drosophila melanogaster*. *J. Exp. Biol.* **217**, 2796–2805 (2014).
18. Billeter, J.-C., Atallah, J., Krupp, J. J., Millar, J. G. & Levine, J. D. Specialized cells tag sexual and species identity in *Drosophila melanogaster*. *Nature* **461**, 987–991 (2009).
19. Zhang, S. X., Rogulja, D. & Crickmore, M. A. Dopaminergic circuitry underlying mating drive. *Neuron* **91**, 168–181 (2016).
20. Ribeiro, I. M. A. et al. Visual projection neurons mediating directed courtship in *Drosophila*. *Cell* **174**, 607–621.e18 (2018).
21. Wu, M. et al. Visual projection neurons in the *Drosophila* lobula link feature detection to distinct behavioral programs. *eLife* **5**, e21022 (2016).
22. Otsuna, H. & Ito, K. Systematic analysis of the visual projection neurons of *Drosophila melanogaster*. I. Lobula-specific pathways. *J. Comp. Neurol.* **497**, 928–958 (2006).
23. Scheffer, L. K. et al. A connectome and analysis of the adult *Drosophila* central brain. *eLife* **9**, e57443 (2020).
24. Talay, M. et al. Transsynaptic mapping of second-order taste neurons in flies by trans-Tango. *Neuron* **96**, 783–795.e4 (2017).
25. Namiki, S., Dickinson, M. H., Wong, A. M., Korff, W. & Card, G. M. The functional organization of descending sensory-motor pathways in *Drosophila*. *eLife* **7**, e34272 (2018).
26. Schretter, C. E. et al. Cell types and neuronal circuitry underlying female aggression in *Drosophila*. *eLife* **9**, e58942 (2020).
27. Rayshubskiy, A. et al. Neural circuit mechanisms for steering control in walking *Drosophila*. Preprint at https://doi.org/10.1101/2020.04.04.024703 (2020).
28. Heisenberg, M. & Wolf, R. *Vision in* Drosophila: *Genetics of Microbehavior* (Springer, 1984).
29. Land, M. F. & Collett, T. S. Chasing behaviour of houseflies (*Fannia canicularis*): a description and analysis. *J. Comp. Physiol.* **89**, 331–357 (1974).
30. Wehrhahn, C., Poggio, T. & Bülthoff, H. Tracking and chasing in houseflies (*Musca*): an analysis of 3-D flight trajectories. *Biol. Cybern.* **45**, 123–130 (1982).
31. Soto-Yéber, L., Soto-Ortiz, J., Godoy, P. & Godoy-Herrera, R. The behavior of adult *Drosophila* in the wild. *PLoS ONE* **13**, e0209917 (2018).
32. Trivers, R. in *Sexual Selection and the Descent of Man, 1871–1971* (Aldine, 1972).
33. Kohatsu, S., Koganezawa, M. & Yamamoto, D. Female contact activates male-specific interneurons that trigger stereotypic courtship behavior in *Drosophila*. *Neuron* **69**, 498–508 (2011).
34. Tinbergen, N. *The Study of Instinct* (Clarendon, 1951).

Methods

Data reporting

Preliminary experiments were used to assess variance and to optimize behavioural conditions. Experiments were not randomized, and the experimenters were not blind to conditions. Sample sizes were not predetermined. For tethered courtship assays, unless otherwise noted, only experiments during which animals exhibited courtship towards the visual targets were included for analysis, selected based on a tracking index >0.3 for at least 1 s and the presence of at least one unilateral wing extension. For modelling of free behaviour, only flies that courted for >90% of the time before copulation were included. For wide-field motion experiments, only flies that exhibited an average optomotor response of at least 5 rad/s were included.

Fly stocks and husbandry

Flies were housed under standard conditions at 25 °C on a 12-h light–dark cycle, except for flies expressing channelrhodopsin variants, which were dark-reared. Fly stocks used were as follows: *Split-P1 GAL4*[15] (D. Anderson, California Institute of Technology); *LC10a GAL4*[20], *LC10a-LexA*[20], and *LC10a-LexA, UAS-CsChrimson:tdTomato;LexAop-GCaMP6m*[20,35,36] (I. Ribeiro and B. Dickson, Janelia Research Campus); *UAS-GtACR1*[37] (A. Claridge-Chang, Duke-NUS); *20X-UAS-CsChrimson.mVenus*[35] (V. Jayaraman, Janelia Research Campus); and *R;Trans-Tango*[24] (G. Barnea, Brown University). The following stocks were obtained from the Bloomington *Drosophila* Stock Center: CantonS, *20XUAS-IVS-jGCaMP7f*[38] (BDSC 79031), *20XUAS-IVS-GCaMP6s*[36] (BDSC 42746), and *OL0019B*[21] (BDSC 68336). *LC10b/c-GAL4*[21] (*GMR_OL0023B*) and *LC10d-GAL4*[21] (*JRC_SS03822*) were obtained from the Janelia Fly Bank.

Supplementary Table 1 provides detailed descriptions of all genotypes used in each experiment.

Behavioural definitions

Here for clarity, we explicitly define the terms used to describe different states in our study based on the behavioural statistics of a courting male. See also Extended Data Fig. 3b.

Arousal: A period during which males exhibit an increased probability of engaging in courtship following spontaneous or exogeneous activation of P1 neurons. Males may or may not engage in courtship continually throughout a period of arousal. 'Unaroused' males do not exhibit any propensity to court visual targets.

Disengagement: A behavioural state adopted by aroused animals when courtship drive becomes very low, during which the visual target fails to elicit behavioural responses completely. Disengagement could not be distinguished from unarousal by behavioural kinematics but was instead inferred post hoc from the fact that males later reinitiated courtship.

Free behaviour assays

All assays were performed with male and virgin female flies 3–5 days after eclosion. Flies were isolated 4–12 h after eclosion and reared with flies of the same sex at low density (5–10 animals) in food vials (d = 3 cm, h = 9 cm) for 3–4 days. Courtship assay chambers were custom-milled bowls with a 38.5-mm diameter, 3-mm depth, and sloped edges to prevent flies from walking upside-down. Chambers were covered with a thin sheet of clear acrylic to prevent flight. Flies were added to the chamber by aspiration without anaesthetic and videos were then recorded for 30 min with a Point Grey FLIR Grasshopper USB3 camera (GS3-U3-32S4M-C: 3.2 MP, 121 FPS, Sony IMX252, Monochrome) using the Flycapture2 Software Development Kit (FLIR). Videos were captured from underneath the chamber at 40 frames per second and with a resolution of 34 ± 1 pixels per micrometre. All behavioural assays were conducted in a heated, humidified room (25 °C, 46% average relative humidity) on a back-lit surface (Logan Electric Slim Edge Light Pad A-5A, 5400K, 6 klx). The x–y coordinates and orientations of the male and female flies were tracked using the Caltech FlyTracker[39]. The angular position of the female target in the male's visual field was calculated using a custom MATLAB (MathWorks) script wherein, for each frame, the male and female x–y coordinates and orientations were translated and rotated such that the male was situated at the origin, facing zero degrees. The angular position of the female was then calculated as the inverse tangent of her y-coordinate over her x-coordinate in this new basis.

Fly tethering and dissection

Flies used for closed-loop behavioural assays were briefly (<30 s) anaesthetized on CO_2, and subsequently tethered to a stainless-steel insect pin (size 00, d = 0.3 mm, l = 4 cm, Fine Science Tools) by their thorax. Anaesthetized flies were placed on a custom-milled plate and held in place by a short string across the neck, and an insect pin was brought in and centred on the back of the thorax. A small dollop of UV-curable glue (Loctite AA 3106) was manually placed at the contact point and cured with a UV gun for 0.5 s. Flies were left to recover from anaesthesia for 1–4 h in a dark chamber humidified by a small wet paper towel.

For open-loop behavioural assays and two-photon functional imaging, flies were briefly anaesthetized on CO_2 and tethered to a custom-milled plate similar to those used in previous studies[9,40]. Flies were held in place by a string across the neck and fixed to the holder by both eyes and the back of the thorax using UV-curable glue (Loctite 3106). To minimize brain motion during functional imaging, the proboscis was also glued to the mouthparts. The string was subsequently removed, and flies were left to recover in a warm, humidified chamber (25 °C, 50–70% humidity) in the dark. For behavioural experiments, flies were transferred to the ball after 2–6 h. For functional imaging experiments, flies were left in the dark until immediately before the assay, at which point the cuticle was removed to give optical access to the central brain without anaesthesia. The tethering plate was filled with saline (108 mM NaCl, 5 mM KCl, 2 mM $CaCl_2$, 8.2 mM $MgCl_2$, 4 mM $NaHCO_3$, 1 mM NaH_2PO_4, 5 mM trehalose, 10 mM sucrose, 5 mM HEPES, pH 7.5 with osmolarity adjusted to 265 mOsm) to cover the fly's head, and the cuticle between the eyes was cut with a 30-gauge needle and removed with forceps. The trachea covering the top of the central brain was removed from both hemispheres with forceps. Flies were subsequently transferred to the ball and left to recover in darkness for at least 30 min.

Virtual reality preparation

For our virtual courtship preparation, we adapted an existing hardware design for presenting tethered flies with visual stimuli (Weisman, J. L. & Maimon, G., personal communication). Male flies rested on a small 6.35-mm diameter ball shaped from Last-A-Foam FR-4618 (General Plastics)[41,42] painted manually with uneven black spots using a Sharpie pen. The Styrofoam ball was held by a custom-milled aluminium base with a concave hemisphere of 6.75 mm. A 1-mm tract drilled through the base connected to air supplied at ~0.8 l/min. The aluminium base was held in place by a custom printed (Carbon 3D) contraption. The ball was illuminated by infrared LED flood lights, and imaged with a Point Grey FLIR Firefly camera (FMVU-03MTM-CS) with a 94-mm/1× WD Video Lens (InfiniStix) by way of a mirror (ThorLabs #ME05-G01). The ball was surrounded by a 270° conical screen with a large diameter of ~220 mm, a small diameter of ~40 mm, and a height of ~60 mm. The screen was cut from matte white 80-lb cardstock (Desktop Publishing Services, Part 59421-50) using a laser cutter and fitted into a custom 3D-printed screen-holder with a tilted slit for placing and forming the screen shape (Extended Data Fig. 1).

The visual stimulus was projected around the male from a DLP 3010 Light Control Evaluation Module (Texas Instruments). During optogenetic behavioural assays (for example, Fig. 1b–f), light was projected by way of a 40 × 40-cm mirror (First Surface Mirrors, custom cut) from above the fly, whereas it was rear-projected onto the front of the screen during all other behavioural experiments and for two-photon calcium

imaging due to the sterics of the objective (Extended Data Fig. 1b). The red and green LEDs in the projector were turned off using the DLP Display and Light Control EVM GUI (Texas Instruments), leaving only the blue LED. The lens of the projector was also covered by blue filter-paper (Rosco). Together, this minimized any aberrant activation of neurons in animals expressing the light-gated cation channel CsChrimson, as split-P1 > CsChrimson flies did not initiate courtship spontaneously when only the blue LED was on. As males walked on the spherical treadmill, all three rotational axes of the ball were read-out by the FicTrac2.0 software[43] at 60 Hz in real time. FicTrac was linked by a socket to MATLAB, which read out the estimated angular position of the ball at each frame. The projector received input from the same computer running FicTrac via an HDMI cable, and was controlled via a mini-USB cable to the same computer. Visual stimuli were generated in the MATLAB-based ViRMEn software[44] and projected onto the screen using custom perspective transformation functions. On each frame of an experiment, the animal's updated position was read-out in MATLAB, and either stored or used to transform the position of the visual stimulus in the case of closed-loop assays. The net visual refresh rate of the visual stimulus ranged from 47.6 Hz to 58.9 Hz. All other experimental variables were regulated in MATLAB on a single computer interfacing with an Arduino Uno that controlled the LED. Wing-extensions were detectable via the same camera used for ball tracking, but a second camera (Point Grey, FMVU-03MTM-CS) was used for better visual access to the wings during manual scoring of wing-extensions.

Closed loop behavioural assays

All flies used for closed-loop experiments were reared in the dark on sugar-yeast food to prevent low levels of ion-flux through light-gated ion channels during development, as previously described[9]. Male flies were transferred 1–2 days after eclosion to food containing 400 μM all-trans-retinal 48 h before behavioural assays[14] and kept at low density (3–7 males per vial). Pin-tethered male flies were placed at the centre of the ball and left to acclimate to the ball for 30–60 min in darkness before the experiment was started. This also served to bring male arousal to a baseline before optogenetic activation of P1 neurons. The change in the animal's heading and the integrated x–y position of the ball was read out from FicTrac on each frame. This positional information was used to update the animal's position and heading in the virtual ViRMEn world. Thus, when the fly turned clockwise, the world was rotated counter-clockwise, and vice versa, simulating the natural visuomotor coupling of a freely behaving fly. Optogenetic stimulation was delivered by way of the red LED in the projector (4 μW/mm^2 at 600 nm), which consistently drove animals to court. The visual stimulus in closed loop experiments consisted of either (i) a black dot that followed a stereotyped motion pattern, or (ii) a black dot that followed a random trajectory influenced by the male's own motion (Fig. 1b), both presented on a white background with a light-grey floor (Supplementary Video 2).

For the former case (i), the diameter of the dot was such that it occupied ~30° of the screen when positioned 10 mm in front of the animal in the virtual world. This is larger than the size of a natural female at the same distance but allowed us to keep the female some distance away from the male in the virtual world while she could still exhibit a similar angular size to a close-up female. This extra distance between the male and female was important to prevent males from accidentally colliding with the female in the virtual world, as there is no tactile feedback available. Distances in the virtual world were determined such that 1 radian of the ball the fly walked on was equivalent to one virtual unit. The object rotated in a circle around the virtual world, whose diameter was equivalent of 20 cm, with a rotational velocity of ~10°/s.

For the latter case (ii), the diameter of the dot was the same as described above, but the female moved in an unpredictable and pseudorandom pattern. The female target originally moved in a random direction with a constant linear speed of ~30mm/s. At each point, she had a 20% probability of switching her current heading direction to a new heading direction, drawn pseudorandomly from a normal distribution with its mean equalling the current heading and a variance of 35°. After a switch, she was prohibited from switching direction over the course of the next second. To prevent the male from losing the female in the infinite world, the female was softly-bounded around 120 mm away from the male in all directions. If the female reached the edge of this bound, her path was redirected towards the male to attempt to 're-entice' him. To prevent the female from being on top of the male, she was also softly-bounded 10 mm from the male (her turns were biased away from the male's current location). Experiments ranged from 10 to 30 min in duration, but, for consistency, only the first 10 min from each animal was included for further analysis.

Open loop behavioural assays

Optogenetically induced courtship. All flies used for open-loop experiments that expressed channelrhodopsin variants were reared in the dark on sugar-yeast food. Male flies were transferred 1–2 days after eclosion to food containing 400 μM all-trans-retinal 48 h before behavioural assays and kept at low density (3–7 males per vial). After plate tethering, male flies were transferred to a humidified warm chamber to recover from anaesthesia for 2–6 h. Flies were subsequently placed on the centre of the ball and left to acclimate for at least 1 h. This ensured that any remnant arousal caused by activation of P1 neurons during mounting had ample time to decay, and that flies were in a baseline state at the onset of the trials. Two 1.5-mm optic fibres (Edmund Optics) were coupled to two high-power red LEDs (660 nm, LED Engin) mounted on a heat-sink (Ohmite), and placed directly above the head of the fly. P1 neurons were optically activated by a single optical pulse, yielding a net power 8 μW/mm^2 at 600 nm. As the power of the red and green LEDs in the projector was set to zero, flies were presented with a small dark blue dot (ø ~28°, mimicking the angular size of a female fly 2 mm away from the male) on a light blue background. This dot oscillated in a symmetric 75° or 160° arc about the male, at a constant distance (that is, size) and with a constant angular velocity.

For most single-stimulus experiments (see exception below), the visual target oscillated with a velocity such that it completed left–right sweeps at ~1 Hz (75°/s or 160°/s). Flies were presented with the visual stimulus for 60–120 s before optogenetic activation of P1 neurons. This allowed us to examine the flies' baseline responses to the visual target, and ascertain that P1 neurons were not being activated by light from the projector as animals did not initiate tracking during this baseline period. P1 neurons were subsequently transiently activated by a single 3-s continuous optical pulse. Following initial P1 activation, we continued to monitor the animal's motion in response to the visual stimulus for the remainder of the trial (between 9 and 29 min). For consistency, only the first 10 min from each animal was included for analysis.

For stop-and-go motion, the target ceased to move for 500 ms at the centre of the screen on each cycle, and subsequently continued on along its arc path (Extended Data Fig. 11h). For experiments in which two dots of different velocities were presented, trials began with a 1–3-min 'blank' period during which no stimulus was presented, after which a single stimulus appeared for 1–2 min. All males robustly courted the target. A second stimulus was subsequently added to the screen. This stimulus was identical to the first stimulus, but moved at 98% of the velocity (Extended Data Fig. 11i, j). The velocity of the faster dot was 80°/s. When examining model parameters, we continuously activated P1 neurons optogenetically during tethered behavioural experiments, allowing us to measure visual responses from males in a uniformly heightened arousal state (Fig. 4).

Pheromone-induced courtship. Virgin male flies were collected following eclosion and group-reared at low density for 2–3 days before behavioural assays. To prepare the stimulating female abdomen, we removed the wings and legs from a 3–7-day old CantonS virgin female to ensure that the distal portion of the male's forelegs could readily

contact her abdomen. We subsequently manually glued a pin to her dorsal thorax, and attached this pin to a long custom 3D-printed holder designed to fit around the conical screen. The female abdomen was positioned ~1.5 cm and 90° to the right of the male before the trial was started and viewed from the side using an IR-sensitive camera (Point Grey, FMVU-03MTM-CS) equipped with a 94-mm focal length lens (InfiniStix). As during optogenetic activation of P1 neurons, male flies were presented with the visual stimulus for several minutes before being presented with the stimulating abdomen of a conspecific female, allowing us to internally control their baseline response to the visual target. To allow the male to sample the abdomen, the experimenter centred the abdomen in front of the male and gently brought it into contact with the male's foreleg using a micromanipulator (Scientifica). The female abdomen was subsequently returned to its initial position to minimize the extent it blocked the male's field of view.

Visually induced courtship. Virgin male flies were collected 2–8 h after eclosion and single-housed for 42–48 h to increase their motivation to court[8,14,17,19]. All courtship assays were performed at Zeitgeber 0–3 h. After plate tethering, male flies were transferred to a humidified warm chamber to recover from anaesthesia for 1–3 h. Flies were subsequently placed on the centre of the ball and left to acclimate for at least 30 min in the dark. Each trial was initiated by the presentation of a stationary visual target for 60 s to examine the animal's baseline locomotion, after which the visual target began to oscillate. The visual target oscillated in a 75° arc about the animal with a constant angular velocity of ~75°/s, but the angular size of the dot was continuously altered to mimic the dynamics of a natural female during courtship. The angular size was altered by changing the distance between the male and the target in the ViRMEn world. The distance between the male and the target was taken from the inter-fly-distance (IFD) in a courting pair over the course of two minutes of courtship, and at each frame the angular position of the target was scaled by this IFD to give rise to a more dynamic female path. Angular sizes ranged between ~8 and 50°, with the average size being 22.5°. Each stimulus frame was thus unique for approximately 2 min of time, and subsequently repeated until the end of the trial, until it intersected its original position. Experiments ranged from 10 to 30 min in duration, but, for consistency, only the first 10 min from each animal was included for further analysis. Across genotypes, ~70% of male flies spontaneously initiated courtship towards the visual target. Importantly, tethered females (n = 9, data not shown) showed no response to the visual target stimulus, consistent with the sexually dimorphic nature of courtship pursuit.

Optomotor assays. Male flies were isolated 12–24 h after eclosion and single-housed in vials with food for 2–3 days until adulthood. After plate tethering, male flies were transferred to a humidified warm chamber to recover from anaesthesia for 1–3 h. Flies were subsequently placed on the centre of the ball and left to acclimate for at least 30 min in the dark. Wide-field motion stimuli were generated in ViRMEn and consisted of a square-wave grating on a light background with a wavelength of 10° and a rotational velocity of 115°/s. To allow us to compare neuronal activity during optomotor tracking to baseline periods, we interleaved presentations of a static grating with presentations of a moving grating during each trial, with each epoch lasting for 200 s. To approximate the turning responses of courting flies in response to an oscillating target stimulus, the moving grating switched its rotational direction (that is, clock-wise to counter clock-wise) every 1,500 ms.

Interleaved courtship-optomotor assays. Male flies were isolated 12–24 h after eclosion and housed in vials with food containing 400 μM all-trans-retinal 48 h before behavioural assays, kept at low density (3–7 males per vial). After plate tethering, male flies were transferred to a humidified warm chamber to recover from anaesthesia for 1–3 h. Flies were subsequently placed on the centre of the ball and left to acclimate for at least 30 min in the dark. Males were presented with a blank white screen for 60 s, and afterwards interleaved 30-s periods of either an oscillating 'female' target (as described under 'Optogenetically induced courtship') or a wide-field grating stimulus. Wide-field grating stimuli altered between clockwise and anticlockwise rotations (each for a duration of 2 s), spaced by a 3-s 'rest' period during which the grating was stationary. Wide-field motion stimuli were generated in ViRMEn and consisted of a square-wave grating on a light background with a wavelength of 15° and a rotational velocity of 30°/s. After 480 s of assessment of the male's baseline response to both the wide-field motion stimulus and the 'female' target, we optogenetically activated P1 neurons for 300 s with the same preparation described under 'Optogenetically induced courtship' and continued to monitor behavioural responses.

Monocular stimulation. To dissociate a male's behavioural response to progressively versus regressively moving visual targets, we presented the 'female' visual target to only one eye while optogenetically activating P1 neurons (split-P1> UAS-CsChrimson). Males were reared as described under 'Optogenetically induced courtship' and presented with a small dark dot (ø 25°) that moved from an angular position of 35° to the males right or left side to the 0° position right in front of the male, and subsequently back again after a 5-s delay. This stimulus was repeatedly presented, interleaved by 5-s delays, for 600 s while we monitored the male's behavioural response.

Analysis of behavioural assays

Heat maps of turning. Turning was computed on a frame-by-frame basis as the circular distance between the animal's current heading and the animal's heading in the next frame using the MATLAB circular statistics toolbox (v. 1.21.0.0)[45]. Heat maps were constructed by computing the phase length (in frames) of the stimulus and multiplying it by 3 (3PL). All frames were fit into a matrix of size $N \times$ PL. A very small number of remnant frames (typically <0.5% of frames) at the end of the trial, caused by the total frames not being divisible by 3PLN, were discarded from heat maps but included in all other analysis.

Fidelity, vigour, and tracking index. To estimate how well animals were actively tracking the stimulus, we computed both the vigour and fidelity of their pursuit in a sliding time-bin of 180 frames (~3.7 s). We defined the fidelity of a male's pursuit as the correlation between the position of the visual target and the males change in heading (rad/s), and the vigour as the net amount of turning the male exhibited in the direction ipsilateral to the visual target. Because neither of these metrics fully captured male behaviour, we defined a tracking index as the product of the fidelity and the within-animal normalized vigour of pursuit (vigor in the current cycle divided by the maximum vigor observed). This normalization step was done to bound the tracking index between −1 and 1, and to correct for any difference in males' ability to turn on the ball. To compute a tracking index for the optomotor response, we used only the normalized vigour of a male's turning (net amount of turning in the direction of wide-field motion), as turning responses typically lagged a change in motion-direction (making fidelity a poor metric), and used a larger time-bin due to the relatively slower visual stimulus alterations (444 frames, 9.3 s). The tracking index was set to zero in the first and last few frames, as we did not have a sufficient number of frames to compute it.

Classification of behavioural epochs. Courtship was classified as any period where the tracking index exceeded 0.3. To separate periods of general locomotion versus periods of courtship (for example, Fig. 2d) when analysing responses to visual stimuli, we averaged the male's velocity for three stimulus cycles and selected all periods where the average tracking index was greater than 0.3 versus periods where it was less than 0.3 but the male's average linear speed exceeded 5mm/s, or his angular speed exceeded 2 rad/s ('moving'). The threshold value

for the tracking index was selected so as to be above fluctuations in the tracking index during random running (Extended Data Fig. 3d). The threshold for angular and linear speed was selected to be well above the noise of a fly standing still caused by small vibrations in the floating ball (Extended Data Fig. 3e, f). The distribution of angular velocities and linear speeds exhibited by animals in epochs classified as 'moving' or 'courting' is shown in Extended Data Fig. 8a, b.

To examine the behavioural kinematics of animals during times of disengagement versus times of active courtship (Extended Data Fig. 3h, i), we found periods where animals were actively courting (TI > 0.3) to compare with periods where the tracking index was less than 0.3. To ensure that we robustly sampled data from each epoch and not transition periods, only epochs that lasted at least 10 s were included in this analysis. To examine the duration of these pausing bouts versus the duration of courtship bouts (Extended Data Fig. 3g), we used the same thresholds but did not set a minimum amount of time for the bout durations. To quantify the probability of an animal transitioning from courtship into a state of disengagement and vice-versa (Extended Data Fig. 3j, k), we segregated behavioural data into 10-s bins and calculated the number of times that the animal transitioned from courtship into disengagement in the given bin, and divided this number by the total amount of time the animal spent in courtship (that is, number of opportunities it had to transition). This yielded the probability that, in any given second, the animal would transition from one state to the other.

Two-photon functional imaging

Functional imaging experiments were performed with an Ultima two-photon laser scanning microscope (Bruker Nanosystems) with a Chameleon Ultra II Ti:Sapphire laser. All samples were excited at a wavelength of 920 nm, and emitted fluorescence was detected with a GaAsP photodiode detector (Hamamatsu). All images were acquired with a 40× Olympus water-immersion objective with 0.8 NA. To reduce high-frequency noise caused by emitted light from the projector during imaging, we placed a piece of blue-light filter-paper (Rosco) in front of the projector lens, and 3D printed a custom light-shield that fit over the objective to prevent light from entering the brain from above.

After cuticular removal as described above, flies were carefully lowered onto the ball using a micromanipulator (Scientifica) and the shrouded objective was lowered over the brain. We subsequently identified the brain region of interest and centred a small ROI over it, yielding an imaging rate of 7–12 Hz. Power was kept low and we ensured that no pixels were saturated. On rare occasions flies were discarded because the glue holding the proboscis broke loose from the mouthparts, causing severe motion artefacts in the *z*-direction, or because the expression of GCaMP was too weak to detect the neuropil of interest at low imaging power.

LC10 imaging. An ROI was selected to cover the entire AOTu on a single hemisphere at the depth with the broadest axon terminal distribution, roughly the centre of the glomerulus in the superior–inferior axis. Flies were subsequently left to acclimate to the ball for at least 30 min before imaging commenced. The hemisphere targeted for imaging was selected pseudorandomly for each fly to ensure that there were no significant biases in expression between the hemispheres. Trials were structured as described under 'Visually induced courtship'. When temporal specificity was critical (for example, in comparing LC10a responses to turning responses or characterizing receptive field properties), we used the faster jGCaMP7f sensor instead of the brighter GCaMP6s sensor. We observed no differences in the Δgain between experiments using the two sensors (Extended Data Fig. 7f, g). These same protocols were employed for imaging LC10b/c (OL0023B) and LC10d (SS03822) neurons.

During imaging of LC10 axon terminals in animals expressing a channelrhodopsin in P1 neurons, we expressed GCaMP6m under the control of LC10a-LexA[20], a weaker but highly selective driver line[46]. We selected a narrow ROI encompassing the AOTu and avoiding the adjacent lateral protocerebral complex (LPC) due to possible aberrant excitation of P1 neurons expressing CsChrimson. During all experiments involving 'continuous' P1 activation, we first delivered a single 2-s pulse of red light, and subsequently pulsed the red light (0.2 Hz, 100 ms pulse width) and imaged between pulses of light. For experiments where we examined the effect of P1 activation on LC10 signalling and behaviour, we first monitored the baseline response. After a 60-s baseline period the stimulus target began to oscillate dynamically to drive males to spontaneously initiate courtship. Males were allowed to court the target spontaneously for four minutes, after which we continuously activated P1 neurons optogenetically for five additional minutes as the target continued to oscillate. For experiments with two symmetrically opposing targets (Extended Data Fig. 8g–j), we similarly avoided including the LPC in our ROIs. After a 60-s baseline period we began to continuously activate P1 neurons optogenetically, and a single stimulus target began to oscillate for 30 s to monitor the baseline response of LC10 neurons. After these initial 30 s, a second visual target whose angular position was equal and opposite to the first target was added, yielding identical stimulation of both eyes.

For experiments where we monitored the responses of LC10 neurons to a wider panel of visual targets (Extended Data Fig. 10b–i), animals were first presented with a sequence of visual targets in the absence of P1 activation. Each visual stimulus was presented 10 times in each motion direction (left–right and right–left sweeping), separated by a 5-s inter-stimulus interval (ISI). The sequence of visual targets was pseudorandomized. After this baseline panel, we repeated the stimulus presentations in identical order while continuously activating P1 neurons as described above. The stimulus panel consisted of four distinct stimuli: a dark 10° wide sphere sweeping at 75°/s; a dark 25° wide sphere sweeping at 75°/s; a tall dark 10° wide bar sweeping at 75°/s; and a dark sphere that expanded from an initial size of 10° to a final size of 100° with constant angular velocity (20°/s) for 4.5 s.

P1 imaging. An ROI was selected to cover the lateral junction in the medio–lateral and dorsal–ventral axes, below the P1 arch and above the protrusion of the P1 ring[4]. As with LC10a imaging, flies were left to acclimate after ROI selection, and the hemisphere targeted for imaging was altered between experiments. Trials were structured as described under 'Visually induced courtship' or 'Optomotor assays'.

Co-imaging of LC10a and P1. To simultaneously monitor calcium transients in P1 neurons and LC10a neurons, we expressed GCaMP6s under the control of both 71-G01 GAL4 and LC10a GAL4. An ROI was selected to cover the lateral junction as described under 'P1 imaging', but extended to incorporate the ipsilateral AOTu as well. During analysis, separate ROIs were drawn to encompass either the LPC or the AOTu. Trials were structured as described under 'Visually induced courtship'.

Imaging analysis

Image stacks were motion corrected using non-rigid motion correction (NoRMCorre)[47] and were subsequently manually validated for motion artefacts. For each experimental recording, an ROI was drawn in FIJI (ImageJ, NIH) across the entire population of interest containing neuropil (for example, for LC10a imaging, an ROI was drawn around the bundle of axon terminals in the AOTu) and the average fluorescence extracted. Fluorescence was normalized in MATLAB by assuming that the pre-stimulus/pre-courtship epoch represented the baseline fluorescence of the populations of interest. The average fluorescence of first 100 frames (~10 s) of recording were thus used as the baseline (F_0), and $\Delta F/F_0$ was defined as $\Delta F_i/F_0 = (F_i - F_0)/F_0$, where i denotes the current frame. To allow us to compare the shape of the responses of LC10a–d neurons during courtship and during plain running, we normalized the average response to one stimulus cycle of each animal to its maximum value across all stimulus cycles in a given behavioural context (that is, $\Delta F_i = \Delta F_i/\Delta F_{max}$).

Image–behaviour correlations. Because imaging data were collected at a lower frame rate than behavioural data, we downsampled the behavioural data using linear interpolation at the imaging time points to allow us to compute correlations between behaviour and imaging. Behavioural data were binned, and the imaging frames corresponding to each bin were averaged. To correlate the fluorescence of LC10a–d neurons with the fly's turning (Fig. 2f), we convolved the fly's heading signal by an exponential with dynamics closely resembling that of jGCaMP7f (rise $\tau = 105$ ms, decay $\tau = 170$ ms)[38] to account for the delay introduced by the calcium sensor. When calculating the average evoked response of LC10a to the visual stimulus, we averaged the responses of all stimulus cycles during courtship and 'moving' (determined as described above) and found the peak $\Delta F/F_0$ of this averaged response for each animal. For computing the gain, we divided the peak–trough difference during running by the peak–trough difference during courting. For computing the correlation between evoked LC10 responses and evoked turning or speed (Extended Data Figs. 8c–f, j, 10g, h) we computed the average maximum evoked response when the stimulus was ipsilateral to the imaged AOTu, as well as the average (or total) turning and linear speed of the animal in the same time period.

To assess the activity of P1 neurons in the different behavioural epochs of a courtship trial (Fig. 1m), we segregated the data into three categories: periods during which animals were actively courting (TI >0.3), periods during which the animal had previously courted and would court at least once more during the trial ('disengaged' periods), and the period before animals initiated courtship. To ensure that we robustly sampled data from each epoch and not transition periods, only epochs that lasted at least 10 s were included in analysis. To analyse how the relationship between P1 activity and behaviour changed over time, we took two approaches: (1) we scatter-plotted P1 activity against the tracking index in the first minute of courtship versus the remainder of the trial (Extended Data Fig. 5c); and (2) we segregated the trial into 30-s bins and computed the correlation between P1 and the tracking index, the maximum P1 activity, and the maximum tracking index in each bin (Extended Data Fig. 5e–g).

To compare the relationship between the responses of LC10 neurons in the AOTu and tracking during spontaneous courtship versus during continuous activation of P1 neurons, we generated 2D density plots of animal's tracking indices against the evoked response of LC10 neurons (Fig. 3g). For each stimulus cycle, we computed the averaged tracking index and the maximum $\Delta F/F_0$ in the AOTu and counted the number of observations in each bin. This was normalized to the total number of observations across animals.

Co-imaging of LC10a and P1 neurons. To analyse the relationship between LC10a activity and P1 neuron activity, we computed the maximum evoked LC10 response each time the stimulus swept across the ipsilateral field-of-view versus the average activity of P1 neurons in the same time period. The responses of each were normalized within animals to account for variations in GCaMP expression (Fig. 3c).

Stimulus panel. To examine the relationship between LC10a activity and ipsilateral turning at differing levels of P1 activity (Fig. 3b), we computed the evoked LC10a activity each time the stimulus swept across the ipsilateral hemifield and versus the total turning of the animal in the direction of the stimulus and the average P1 activity in the same period. To estimate whether P1 neuron activity or LC10a activity occurred first, we computed the cross-covariance of the raw GCaMP signals collected from each neuropil (Extended Data Fig. 10a). Cross covariances were normalized such that the autocovariance at zero lag equalled 1. For computing the cross-covariances, all recordings were linearly interpolated to a common time-basis of 10 Hz to correct for slight variations in imaging rates across animals (images were acquired at 8–12 Hz).

Size-dependence of response. To estimate the extent to which the animal's turning response and the magnitude of the evoked $\Delta F/F_0$ of LC10a neurons depended on the angular size of the stimulus (Extended Data Fig. 8m, n), we computed the average angular size of the target stimulus for each stimulus cycle during visually induced courtship trials, and computed the average behavioural and neural response for each 2° bin of angular sizes.

To examine the responses of LC10 neurons to our panel of stimuli, we computed the average evoked LC10 response for each animal from 2 s before the stimulus started moving to 2 s after it had ceased moving, and plotted the average of these responses across animals. To estimate the magnitude by which responses to the different stimuli were modulated by P1 activation (Extended Data Fig. 10f), we computed a response modulation index as the relative difference between evoked LC10a response during P1 stimulation versus baseline. That is:

$$\mathrm{RMI} = \frac{\mathrm{LC10}_{+\mathrm{P1}} - \mathrm{LC10}_{-\mathrm{P1}}}{\mathrm{LC10}_{+\mathrm{P1}} + \mathrm{LC10}_{-\mathrm{P1}}}$$

Where LC10 denotes the average response in the given condition (with or without P1 activation). This metric is beneficial because it is bounded between −1 and 1, and because it preserves the relative difference between responses with and without P1 activation (for example, a twofold amplification by P1 activation always yields the same value, regardless of the magnitude of the responses).

Direction selectivity of LC10 neurons. To examine the direction selectivity of LC10a neurons across the population, we examined the average evoked LC10a $\Delta F/F_0$ response to progressively versus regressively moving targets in the presence or absence of P1 activation and calculated a direction selectivity index. The direction selectivity index was computed analogously to the response modulation index described above:

$$\mathrm{DSI} = \frac{\mathrm{LC10}_{\mathrm{Progressive}} - \mathrm{LC10}_{\mathrm{Regressive}}}{\mathrm{LC10}_{\mathrm{Progressive}} + \mathrm{LC10}_{\mathrm{Regressive}}}$$

Where LC10 denotes the average response in the given condition (progressive or regressive motion). When the average $\Delta F/F_0$ for an ROI was negative, the average response was set to zero as it would otherwise interfere with calculation of the direction selectivity index.

While LC10 neurons, on aggregate, responded more strongly to progressively moving stimuli than regressively moving ones (Extended Data Fig. 10i), we wondered whether this could be attributable to distinct subpopulations of LC10 neurons, given that this feature was not found by previous studies[20]. To examine the direction selectivity of individual LC10a boutons in the AOTu, we analysed data from the multi-stimulus panel in which animals were presented with 25° sweeping dots, separated by a 5-s inter-trial-interval, during continuous P1 activation. To identify ROIs, we used semi-unsupervised constrained non-negative matrix factorization (CNMF)[48] using a Greedy initialization method on motion-corrected videos (Extended Data Fig. 11a, b). This algorithm is beneficial because it segregates pixels into ROIs according to both their temporal and spatial footprints, identifying contiguous sets of strongly correlated pixels that presumably correspond to the axon boutons of individual LC10a neurons. It can also extract components with overlapping spatial footprints. A small number of ROIs were manually discarded because they labelled regions outside of the AOTu where no GCaMP was expressed.

Two-photon optogenetic stimulation

Activation. For targeted activation of LC10a neurons in LC10a>UAS-CsChrimson animals, animals were placed on the ball and a small 'stimulation' ROI over the AOTu was defined as described above. We subsequently identified a second 'sham' ROI of similar size,

and set the frame rate of both ROIs to 10 Hz. The sham ROI was adjacent to the stimulation ROI and within the same hemisphere, but did not include any fluorescent neuropil. After ROI identification, animals were left to acclimate to the ball for at least 1 h before the experiment commenced. During the experiment, we increased the power of the laser to intermediate levels, and switched between focusing the laser over the stimulation ROI and the sham ROI every ~4 s (40 frames plus a 750-ms delay to switch the laser focus) while recording the animal's motion in FicTrac as described above. Animals were in the dark and no visual stimulus was presented. Each trial lasted 10–30 min, but only the first 10 min were included in analysis for consistency.

Silencing. For targeted silencing of LC10a neurons in LC10a > UAS-GtACR1 flies, we selected a sham ROI and a stimulation ROI as detailed above. Note that only one *z*-slice of the AOTu was targeted, making two-photon silencing less profound than broad optogenetic silencing but exquisitely spatially targeted, allowing us to focus on one hemisphere without affecting the other. After resting, trials were structured as described under 'Visually induced courtship'. The laser was focused over the sham ROI during the first stimulus oscillations to ensure that animals properly initiated courtship, and subsequently moved between the stimulation ROI and the sham ROI every 60–90 s for the duration of the trial to intermittently silence LC10a neurons in one hemisphere. As with activation, the first 10 min of each trial were included in analysis.

Model of turning dynamics

We constructed a network model of the visuo-motor transformation underlying animal's behavioural responses to small moving targets during courtship. The core of the model consists of 20 LC10a neurons per hemisphere, modelled as leaky integrate-and-fire units with spike-rate adaptation[49]. Membrane voltage was computed as:

$$\tau_m \frac{dV}{dt} = V_{Rest} - V - R_m g_{sra}(V - E_{K^+}) + R_m I_e$$

with a membrane time constant (τ_m) of 10 ms, a resting membrane voltage (V_{Rest}) of −65 mV, a membrane resistance (R_m) of 10 MΩ, and a potassium reversal potential (E_{K^+}) of −70 mV. The threshold for spiking is −50 mV, after which the membrane voltage is reset to V_{Rest}. The spike rate adaptation is modelled as a potassium conductance (g_{sra}), which increases with each spike in the unit, such that $g_{sra} = g_{sra} + \Delta g_{sra}$, where $\Delta g_{sra} = 14$ nS. The potassium conductance is altered such that:

$$\tau_{sra} \frac{dg_{sra}}{dt} = -g_{sra}$$

It thus decays to exponentially zero with a time constant $\tau_{sra} = 200$ ms. The system of equations was estimated over the entire duration of the trial using Euler's method with a time-step of 3 ms. The input to the model was the angular position of the target stimulus, updated at the same framerate as it was presented to animals (~50 Hz).

In each hemisphere, each LC10a neuron covers a non-overlapping region of space. Because stimuli were presented only to the front of the male during tethered behaviour, the modelled field of view ranged from 0° to 180° with 15° of binocular overlap[28] (that is, each neuron coved 10.5° of the visual field). Each neuron was sensitive to motion only in its designated field of view and was assumed to be completely selective for progressive motion, with zero response to regressive motion. Importantly, model neurons were sensitive to the change in the angular position of moving objects, but not their angular size on the retina, consistent with the broad tuning of LC10a receptive fields and behavioural evidence that males track targets of varying size with equivalent vigour during close-range pursuit[20] (Extended Data Fig. 8m, n).

To compute the input current to each unit of the model, we transformed the estimated temporal receptive fields of LC10a neurons[20] into a continuous equation by fitting softmax functions to the rising and falling phase independently, and subsequently multiplying the two (Fig. 4a):

$$RF = \frac{1}{(1 + e^{\beta(t-\alpha)})(1 + e^{-\sigma(t+\kappa)})}$$

where t indicates the time at which motion occurred. Values $\kappa = 0.849$, $\sigma = 5.527$, $\alpha = -0.186$, and $\beta = 15.588$ provided the best fit to the estimated receptive field according to a grid search. Note that the product of the softmax functions is bounded between zero and one, and thus provided only the relative structure of the receptive fields. To compute the total amount of input current to LC10a neurons in a given moment, we summed up this equation for all periods in time during which visual motion had occurred in the model neuron's spatial receptive field, and scaled it by a constant factor S_f such that:

$$I_e = S_f \sum_{i=1}^{N} \frac{1}{(1 + e^{\beta(t_i-\alpha)})(1 + e^{-\sigma(t_i+\kappa)})}$$

where S_f was set to 1.5 nA. As indicated, the total input current was the sum of the receptive fields up to the current time point, multiplied by the scaling factor. Input was thus primarily driven by visual motion that occurred in the past 500 ms, and visual motion that occurred further than ~2 s ago yielded essentially no input current in accord with the estimated receptive fields. Neurons only received input from the time points where the stimulus was present in the neuron's spatial receptive field.

Modelling free behaviour. To model turning responses of freely behaving animals in response to female motion, we selected courtship assays during which the male courted the female for at least 90% of the time before copulation. This ensured that our model was primarily compared to the male's behaviour during active, close-range courtship. To generate input, we estimated the position of the female on the male's retina for each frame as a point as described above and provided this positional information to the model to generate turning. Because the female could occupy any position relative to the male in this preparation, we modelled the full estimated 270° field-of view with 15° of binocular overlap[28], and slightly increased the visual resolution of the model so that each LC10a model neuron covered only 7.5° of visual space (40 model neurons total). Because this caused each unit to receive less input current (as the stimulus spent less time within each receptive field), we also increased S_f to 2.5 nA to compensate.

To model pursuit in 2D space (Supplementary Video 7), rather than turning responses alone, we initialized the model with the same heading and position as the real male and provided the initial angular position of the female relative to the model. On each frame of the video recording, we updated the angular position of real female fly, and allowed the model to reorient proportionally to the firing rate in the left and right LC10a populations (with a net 200 spikes equalling a 1-rad turn). To move the model in two dimensions and allow it to keep up pace with the female, we displaced the model by the same magnitude as the female on each frame, oriented in the direction of the model's heading. The only exception to this displacement was when the female exhibited an instantaneous velocity less than 2.5 mm/s, at which point the model reoriented but was not displaced in 2D space.

Notably, from this initialization of the model and onwards, the real male and the model were completely decoupled from each other, and independently pursued the target along similar trajectories. In computing the cross covariance between the model and male behaviour, we normalized cross covariances such that the autocovariance at zero lag equalled 1.

Incorporating P1 activity. To incorporate the fluorescence of P1 neurons, we de-noised the $\Delta F/F_0$ time series[50] and corrected for any drift in

the baseline fluorescence using a sliding percentile filter with a window size of 200 s. To modulate the responses of LC10a neurons in our continuous model, we simply multiplied the input current I_e by the $\Delta F/F_0$ recorded in the closest previous imaging frame. In our threshold-based model, we set a threshold limit of 0.15 $\Delta F/F_0$ (approximately 3σ of the baseline $\Delta F/F_0$ distribution of P1 neurons). When the fluorescence of P1 neurons exceeded this limit, the model received strong input (equivalent to 0.5 $\Delta F/F_0$ in the continuous model); when it did not, the model received no input on the given frame.

Analysis of model results

To transform spiking in LC10a model neurons to estimates of turning, we implemented a contralateral inhibition component in which we subtracted the number of spikes from LC10a neurons in the left hemisphere from that of LC10a neurons in the right hemisphere in discrete time bins of 30 ms. The model turned in the direction with the highest net number of spikes in the given bin, scaled by the magnitude of the net number of spikes. The model was aimed at capturing the dynamics of turning during courtship and the relative magnitude of turns. The absolute magnitude of turning to which each spike corresponds in the courting animal is an unconstrained problem and subject to the magnitude of the scaling factor S_f. For P1 incorporation and during free behaviour we found that a net 300 spikes/s corresponded to roughly 1 rad/s. These values were used for converting spikes to estimated turning (for example, Fig. 4e).

Each representative alignment of the model and behaviour was replicated across at least four animals. For computing the Pearson correlation or the cross-correlation between the model's predicted turning and the animal's actual turning, we downsampled the model net spiking data using linear interpolation at the behavioural time points, because the model frame rate was several times faster than the behavioural recording rate. The animal's heading signal was smoothed using a moving average window of 30 ms. To estimate the fraction of turns that was accurately predicted by the model (Extended Data Fig. 13a; the model 'hit' rate) we detected all cycles during which the animal executed an ipsiversive turn of at least 2 rad and calculated the fraction of these peaks that were accompanied by a model in the same direction. To estimate the fraction of turns that the model took but the animal did not take (Extended Data Fig. 13a; the model 'false alarm' rate), we similarly detected all ipsiversive model turns of at least 1 rad, and calculated the fraction of these peaks that were accompanied by an animal turn of at least 1 rad in the same direction. The threshold for detecting a turn was lower for the model because it, unlike behaviour, is effectively noiseless.

To estimate the importance of the temporal structure of the LC10a receptive fields, we varied the κ parameter in the input function of our model to yield faster or slower rise-times and compared the Pearson correlation between the model and animals over a 60-s period of courtship (Extended Data Fig. 11g). This variation in the receptive fields causes a narrowing or broadening of the receptive fields, with smaller rise-times yielding less net excitatory input to the model and vice-versa. To correct for this variation, we normalized the area under the curve of the receptive fields by that of the standard model described above (that is, $\kappa = 0.849$).

To compute the turning responses of animals and the model for varying levels of P1 activity, we computed the total turning in the direction of the target stimulus for each stimulus cycle, and binned these turning responses based on the maximum $\Delta F/F_0$ exhibited by P1 neurons in the same stimulus cycle.

Analysis of the female hemibrain connectome

Identifying LC10 subtypes. We analysed the skeletons and synapses of traced neurons in the female adult hemi-brain connectome (hemibrain: v1.2)[23] using the Neuprint toolkit in R[51]. In the connectome, 449 neurons have been labelled as LC10 neurons, but the four subtypes (a–d) of LC10 neurons[21,22] have not been separated. To separate these, we manually inspected each of the LC10 neurons and designated each of them as LC10a, LC10b, LC10c, LC10d, or unknown. We payed particular attention to the location of the soma, the branching structure of dendrites in the lobula, the depth of dendritic branches in the lobula, and the branching structure of axons in the large subunit of the AOTu. We were highly selective in our designation and thus denoted roughly half of LC10 neurons as unknown when we could not ascertain the cell-type based on morphology. We repeated this process twice and designated neurons as belonging to a cell-type only when it was independently identified on both rounds. In total, we identified 59 LC10a neurons, 44 LC10b neurons, 66 LC10c neurons, and 80 LC10d neurons. The Neuprint ID number for each of these neurons is given in Supplementary Table 2.

Analysis of LC10 synaptic connectivity. To examine the differences in presynaptic and postsynaptic partners of the different LC10 subtypes, we first computed the correlation between the output/input vectors for all pairs of labelled LC10 neurons. The sorted correlation matrices for inputs and outputs are shown in Extended Data Fig. 9c, e. Second, we visualized differences in the output and input connectivity matrices using *t*-distributed stochastic neighbour embedding (t-SNE) with a perplexity of 30, and labelled individual LC10 neurons according to their subtype. To group outputs of LC10a neurons by brain region, we examined each of the postsynaptic partners of all LC10a neurons and identified the three brain regions that these partners innervated most densely, on the basis of total presynaptic counts. To group inputs, we examined each of the presynaptic partners of LC10a neurons and identified the three brain regions in which these partners received the most input on the basis of total postsynaptic counts. Brain regions were defined according to standard meshes included in the hemibrain data set. We excluded connections from or to optic neuropils, and brain regions to which LC10a neurons were connected to by fewer than 50 synapses in total across the whole population (for example, LC10a neurons form only 27 synapses with postsynaptic partners projecting to the bulb (BU), and this connection was thus not plotted). The full brain-region connectivity is included in Supplementary Table 2. We plotted the full morphology only of neurons that were strongly connected to LC10a neurons, as assessed by the existence of at least 10 synaptic connections between an LC10a neuron and the connected neuron. These were grouped manually as projecting to either the lateral accessory lobes or the inferior bridge.

Trans-tango and immunohistochemistry

The *LC10a* GAL4 line used for all other experiments also labels a sparse number of Kenyon cells[20], which is amplified to label many Kenyon cells by the trans-Tango expression system[24]. To visualize the downstream synaptic partners of LC10a, we instead used a sparser split-GAL4 line that exclusively labels LC10a neurons (OL0019B)[21]. This line was not used for functional imaging experiments owing to low expression levels. OL0019B > R; trans-Tango males were selected 8–12 h after eclosion and group housed at medium density (15–20 flies per vial). To allow proper expression, males were aged for 30–40 days at 20 °C before dissections. Brains were dissected in Schneider's medium (Sigma Aldrich S0146) for 30 min and then immediately transferred to cold 1% paraformaldehyde (Electron Microscopy Sciences) and fixed for 16–20 h at 4 °C. Samples were then washed in PAT3 buffer (0.5% BSA, 0.5% Triton X-100, 1X PBS, pH 7.4) three times. The last two washes were made by incubating samples for 1 h on a nutator at room temperature. A 3% goat serum block was added, and brains were incubated on a nutator for 90 min at room temperature before the block was removed and 1 ml of fresh 3% goat serum was added back, along with primary antibodies. Primary antibodies used were 1:50 mouse anti-Brp (nc-82, Developmental Studies Hybridoma bank), 1:1,000 rabbit anti-GFP (A11122, Invitrogen; against OL0019B > UAS-myrGFP), and 1:100 rat anti-HA (11867423001, Roche; against QUAS-mtdTomato). Brains were incubated with primary

antibodies on a nutator for 3 h at room temperature, and then moved to a nutator at 4 °C for 12–16 h. Samples were subsequently washed three times with PAT3 buffer as detailed above. The final wash was removed and 1 ml of fresh 3% goat serum added along with secondary antibodies. Secondary antibodies used were 1:500 AF555 goat anti-rat (A21434, Invitrogen), 1:500 AF633 goat anti-mouse (A21052, Invitrogen), and AF488 goat anti-rabbit (A11034, Invitrogen). Samples were incubated with secondary antibodies for 4 days at 4 °C on a nutator, and subsequently mounted in Vectashield (Vector Laboratories) in 5/8th-inch hole reinforcements placed on glass slides. Images were captured on an inverted Zeiss LSM 780 confocal microscope using a 25× objective.

Statistics and reproducibility

Please see Supplementary Table 1 for details on statistics. All statistical analyses were performed in MATLAB R2019a or GraphPad Prism 9. Datasets were tested for normality using the Shapiro–Wilk method, and appropriate statistical tests applied as described in Supplementary Table 1 (for example, *t*-test for normally distributed data, Fischer's exact test for categorical observations, Mann–Whitney *U*-test for non-parametric data, Friedman test with Dunn post hoc test for non-parametric data with repeated measurements). All statistical tests used were two-tailed. Our model was noise-less and thus fully deterministic. Shaded regions surrounding line-plots indicate ± s.e.m. unless otherwise stated. Experimenters were not blinded to the conditions of the experiments during data collection and analysis. All attempts at replication were successful.

Reporting summary

Further information on research design is available in the Nature Research Reporting Summary linked to this paper.

Data availability

All data underlying this study are available upon request from the corresponding author. Source data are provided with this paper.

Code availability

Code underlying the network model is available at https://github.com/rutalaboratory/LC10NetworkModel.

35. Klapoetke, N. C. et al. Independent optical excitation of distinct neural populations. *Nat. Methods* **11**, 338–346 (2014).
36. Chen, T.-W. et al. Ultrasensitive fluorescent proteins for imaging neuronal activity. *Nature* **499**, 295–300 (2013).
37. Mohammad, F. et al. Optogenetic inhibition of behavior with anion channelrhodopsins. *Nat. Methods* **14**, 271–274 (2017).
38. Dana, H. et al. High-performance calcium sensors for imaging activity in neuronal populations and microcompartments. *Nat. Methods* **16**, 649–657 (2019).
39. Eyjolfsdottir, E. et al. Detecting social actions of fruit flies. In *Computer Vision — ECCV 2014* (eds. Fleet, D., Pajdla, T., Schiele, B. & Tuytelaars, T.) vol. 8690, 772–787 (Springer, 2014).
40. Maimon, G., Straw, A. D. & Dickinson, M. H. Active flight increases the gain of visual motion processing in *Drosophila*. *Nat. Neurosci.* **13**, 393–399 (2010).
41. Green, J. et al. A neural circuit architecture for angular integration in *Drosophila*. *Nature* **546**, 101–106 (2017).
42. Seelig, J. D. & Jayaraman, V. Neural dynamics for landmark orientation and angular path integration. *Nature* **521**, 186–191 (2015).
43. Moore, R. J. D. et al. FicTrac: a visual method for tracking spherical motion and generating fictive animal paths. *J. Neurosci. Methods* **225**, 106–119 (2014).
44. Aronov, D. & Tank, D. W. Engagement of neural circuits underlying 2D spatial navigation in a rodent virtual reality system. *Neuron* **84**, 442–456 (2014).
45. Berens, P. CircStat: a Matlab toolbox for circular statistics. *J. Stat. Softw.* **31**, 1–21 (2009).
46. Nojima, T. et al. A sex-specific switch between visual and olfactory inputs underlies adaptive sex differences in behavior. *Curr. Biol.* **31**, 1175–1191.e6 (2021).
47. Pnevmatikakis, E. A. & Giovannucci, A. NoRMCorre: an online algorithm for piecewise rigid motion correction of calcium imaging data. *J. Neurosci. Methods* **291**, 83–94 (2017).
48. Giovannucci, A. et al. CaImAn an open source tool for scalable calcium imaging data analysis. *eLife* **8**, e38173 (2019).
49. Dayan, P. & Abbott, L. F. *Theoretical Neuroscience: Computational and Mathematical Modeling of Neural Systems* (Massachusetts Institute of Technology Press, 2001).
50. Friedrich, J. & Paninski, L. Fast active set methods for online spike inference from calcium imaging. In *Advances in Neural Information Processing Systems 29* (eds. Lee, D. D., Sugiyama, M., Luxburg, U. V., Guyon, I. & Garnett, R.) 1984–1992 (2016).
51. Clements, J. et al. neuPrint: analysis tools for EM connectomics. Preprint at https://doi.org/10.1101/2020.01.16.909465 (2020).

Acknowledgements We thank K. Kuchibhotla, B. Noro, L. Abbott, S. R. Datta, R. Coleman, and P. Brand for comments on the manuscript; I. Ribeiro for discussions and sharing the LC10a split-GAL4 and LC10a-LexA driver lines; Y. Aso for LexAop-GCaMP6s/UAS-CsChrimson flies; J. Weisman and G. Maimon for sharing their designs for an integrated, projector-based system for presenting tethered, walking flies with visual stimuli in advance of publication; R. Coleman, I. Morantte, A. Siliciano, J. Petrillo, and Rockefeller Precision Instrumentation Technologies for technical advice; and G. Maimon, C. Bargmann, L. Abbott, and members of the Ruta laboratory for discussion. Stocks obtained from the Bloomington *Drosophila* Stock Center, NIH P40OD018537 were used in this study. This work was supported by the Simons Collaboration on the Global Brain, a Reem-Kayden Award, grant 5R35NS111611 from the National Institute of Health to V.R., a David Rockefeller Fellowship and National Science Foundation Graduate Research Fellowship Program to T.H.S., and an HHMI Hanna H. Gray Fellowship to A.O.

Author contributions T.H.S. and V.R. conceived of and designed the study. T.H.S. and R.L. performed tethered behavioural experiments. A.O. carried out the free courtship assays in Fig. 4. T.H.S. performed and analysed functional imaging experiments. T.H.S. designed and implemented the model. T.H.S. and V.R. analysed data and wrote the manuscript with input from R.L and A.O.

Competing interests The authors declare no competing interests.

Additional information

Supplementary information The online version contains supplementary material available at https://doi.org/10.1038/s41586-021-03714-w.

Correspondence and requests for materials should be addressed to V.R.

Peer review information *Nature* thanks Michael Reiser and the other, anonymous, reviewer(s) for their contribution to the peer review of this work. Peer reviewer reports are available.

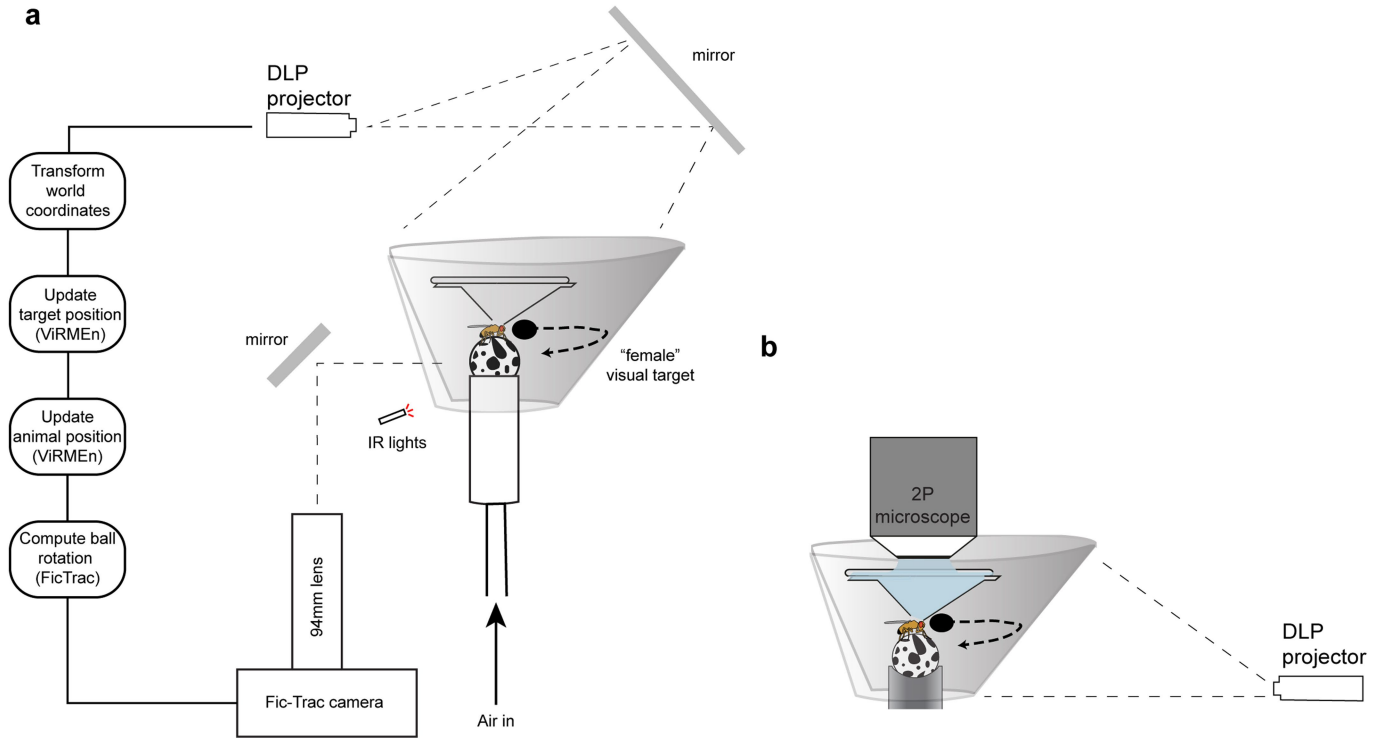

Extended Data Fig. 1 | A virtual reality preparation for tethered courtship. **a**, Schematic of virtual reality preparation. Tethered male flies are placed on an air-cushioned foam ball, whose rotational velocity along all three axes is read out by a single camera via the FicTrac software. During closed-loop experiments, the male's position in the virtual world is updated on the basis of these rotations, as is the position of the target stimulus on the screen. Changes in the 2D world are mapped to a conical screen and projected by way of a mirror from above. Hardware design by J. Weisman and G. Maimon. **b**, Schematic of the stimulus presentation during two-photon imaging. Owing to the sterics of the objective, the stimulus is rear-projected onto the screen instead of being projected from above as in **a**.

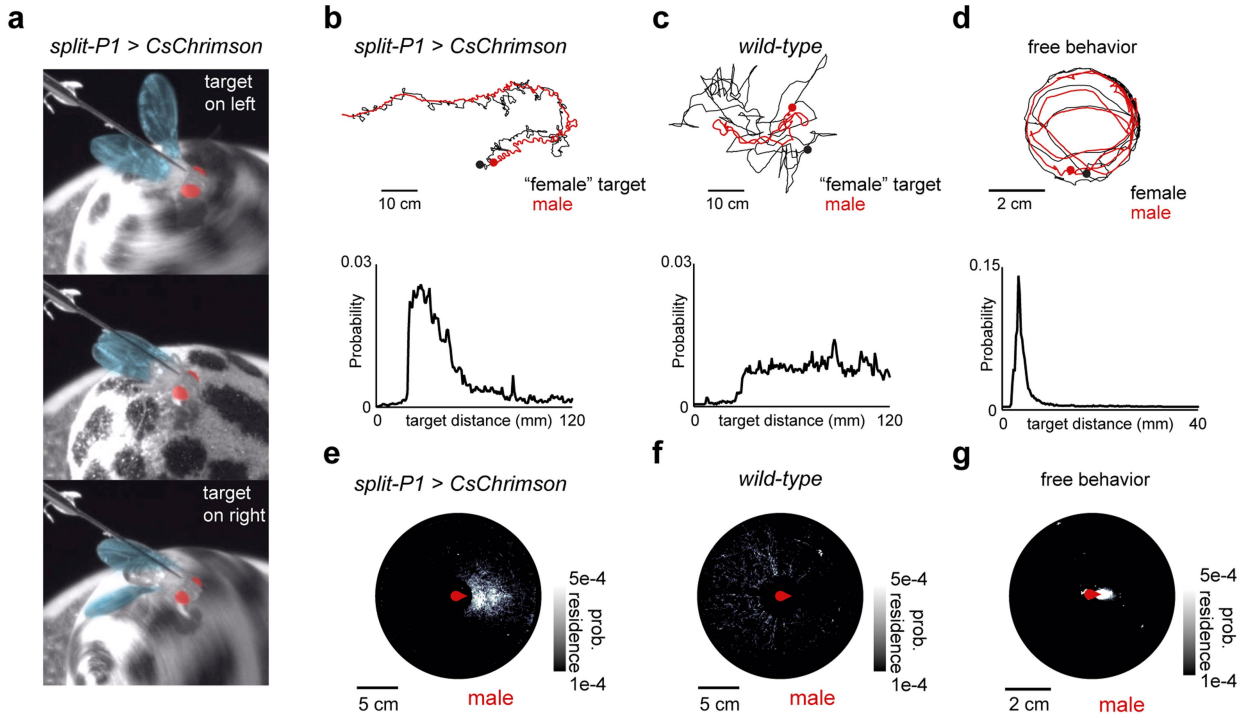

Extended Data Fig. 2 | Tethered courtship in an open 2D virtual world. **a**, Pseudocolour images of a courting male fly during activation of P1 neurons when the visual target is on his left (top), on his right (bottom), or in front of him (middle) showing ipsilateral wing extensions characteristic of courtship song. **b**, Top, position of the male and autonomously moving fictive female in the 2D world during P1 activation over the course of 200 s. Bottom, histogram of the distance between the male and female target during closed-loop courtship. Note that the male is prevented from bringing the stimulus closer than about 10 mm from his position in the virtual world. **c**, As in **b** but for a wild-type male. The increased jitter in the 'female' trajectory results from the target frequently reaching the maximum distance from the male and subsequently approaching him along a straight path. **d**, Top, representative example of the 2D positions of the male and female in a freely courting pair of animals. Bottom, histogram of the distance between the male and female fly. **e**, Density plot of the relative position of fictive females with respect to the courting male during P1 activation. **f**, As in **e** but for a wild-type male. **g**, Density plot of the location of the female relative to the male in freely courting pairs of animals. Details of statistical analyses and sample sizes are given in Supplementary Table 1.

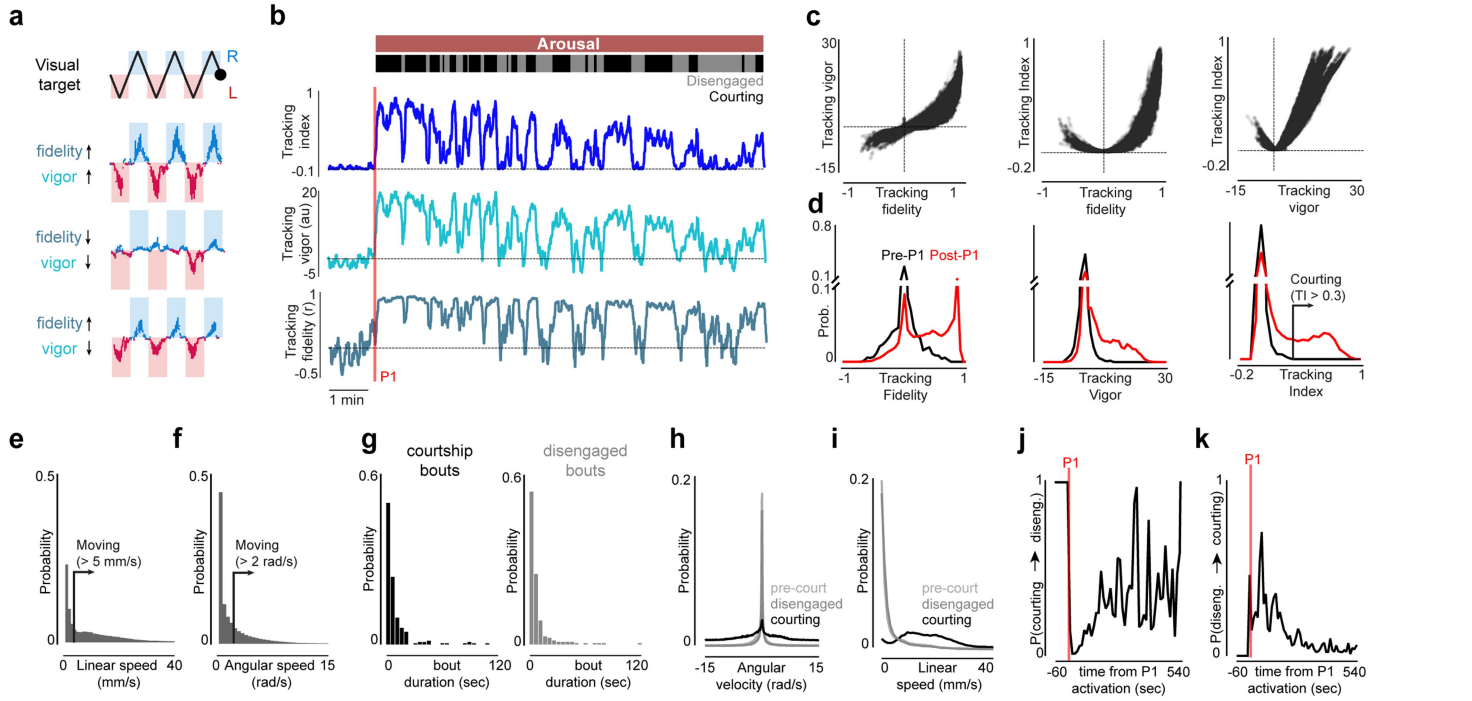

Extended Data Fig. 3 | The behaviour of aroused animals. a, Schematic illustrating our definition of the vigour and fidelity of a male's courtship pursuit. Vigour is quantified as the total turning in the direction of the visual target (normalized within-animal), while fidelity is the correlation between the visual target and the male's turning. **b**, Representative example of the vigour, fidelity, and tracking index over the course of a courtship trial. P1 activation is denoted by red line. The male is classified as courting when TI > 0.3, and as disengaged when TI < 0.3 but he remains primed to reinitiate courtship pursuit. **c**, Comparison of the tracking fidelity, tracking vigour, and tracking index across animals. Each dot represents one frame; black lines indicate zero on axes. **d**, Distribution of tracking fidelity, tracking vigour, and tracking indices across animals, before (black) and after (red) brief activation of P1 neurons. TI > 0.3 was used as a cut-off to indicate courting males. **e**, **f**, Distribution of linear speeds (**e**) and angular speeds (**f**) during courtship trials. Lines indicate the thresholds used for denoting animals as 'moving' (for example, Fig. 3d, e). **g**, Distribution of the duration of bouts of courtship (black) and bouts of disengagement (grey) after transient P1 activation. **h**, Distributions of the angular velocity exhibited by animals that are actively courting (black), that are disengaged (dark grey), or that are passively watching the visual stimulus before P1 activation (light grey). **i**, As in **h** but for linear speeds. **j**, Probability that an animal that is currently courting will transition to disengagement in any given second, plotted over the course of a trial in 10-s bins (red line denotes P1 activation). **k**, Probability that an animal that is disengaged will transition to courtship in any given second, plotted over the course of a trial in 10-s bins (red line denotes P1 activation). Details of statistical analyses and sample sizes are given in Supplementary Table 1.

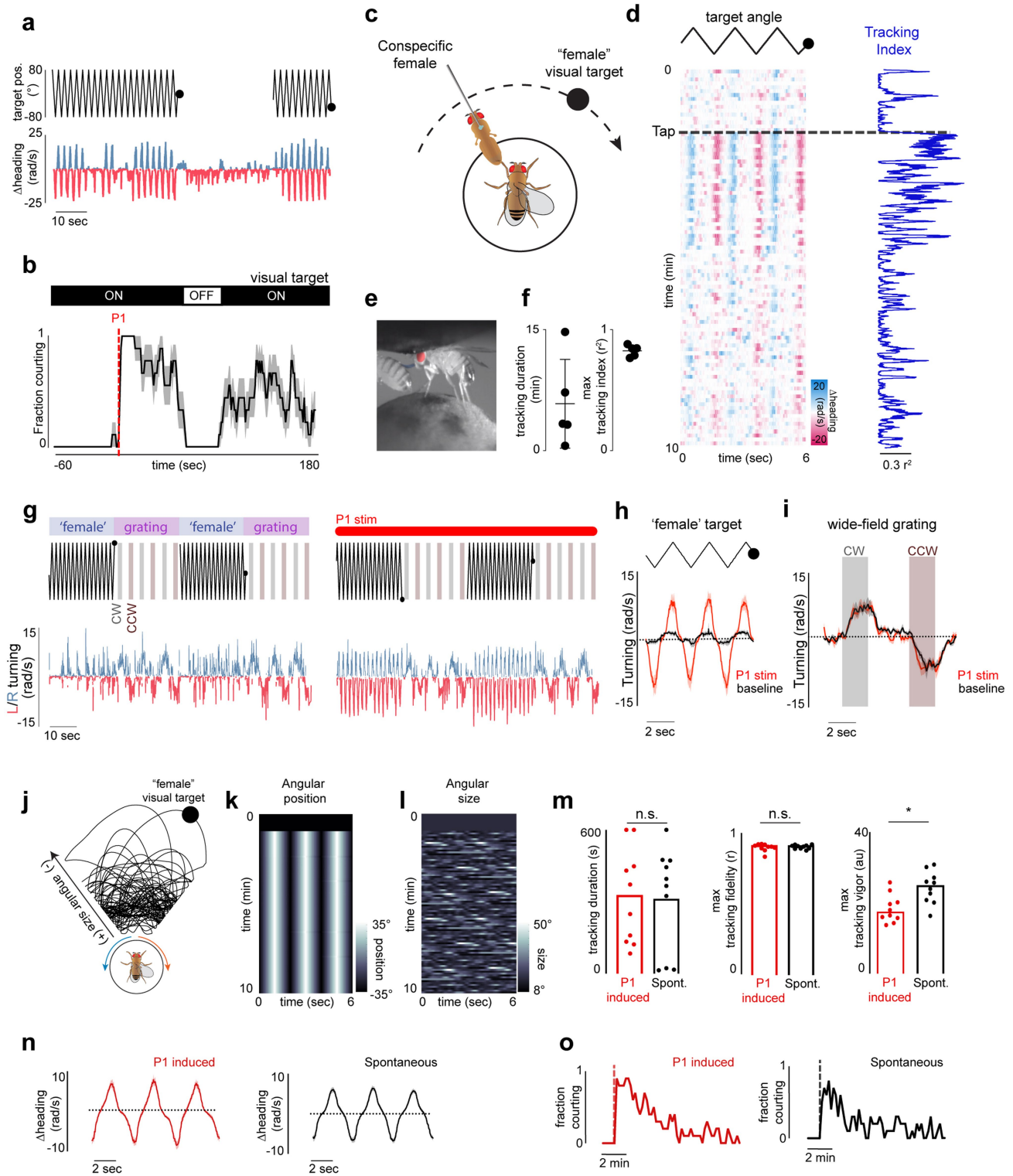

Extended Data Fig. 4 | See next page for caption.

Extended Data Fig. 4 | Acute and enduring regulation of courtship arousal. **a**, Heading of a courting male before, during, and after the visual target was transiently removed from the screen (30 s). Courtship arousal was induced by a 3-s optogenetic activation of P1 neurons expressing CsChrimson 60 s before stimulus removal. **b**, Average tracking index of males during trials where stimulus was removed (mean ± s.e.m.). P1 neurons were transiently activated for 3 s, 1 min after the visual target began to oscillate, and target was temporarily removed from the screen for 30 s 1 min after P1 activation. **c**, Schematic of the preparation allowing male to sample gustatory pheromones to trigger courtship. The male fly was provided with the abdomen of a virgin female to taste with his foreleg while the visual target oscillated on the screen in front of him. **d**, Example of a male's heading during a courtship trial, before and after the male tapped the female abdomen with his foreleg (black line indicates tap). Each row consists of three stimulus cycles. **e**, Pseudocolour image of a male fly sampling the pheromones on a female abdomen. **f**, Maximal tracking index (right) and duration between the first and last detected bouts of courtship (left) during tapping-induced courtship trials. **g**, Representative example of male turning during interleaved presentations of either a female target (black line) or a wide-field grating turning in the clockwise (CW, grey) or anticlockwise (counterclockwise; CCW, burgundy) before (left) or during (right) optogenetic activation of P1 neurons. **h**, Average male turning in response to three cycles of the oscillating female target before (black) or during (red) activation of P1 neurons. **i**, Average male turning in response to the wide-field grating rotating in the clockwise (grey) or anticlockwise (burgundy) direction before (black) or during (red) activation of P1 neurons. Note that unlike responses to the 'female' target in (**h**), optomotor responses were not enhanced during P1 activation. **j**, Two-dimensional path of the dynamic visual target used for inducing spontaneous courtship. **k**, **l**, Angular position (**k**) and angular size (**l**) of the dynamic visual target subtended on the male retina over the course of a 10 min trial. **m**, Duration between the first and last detected bouts of courtship for trials induced by optogenetic activation of P1 neurons or spontaneously initiated (left), and the maximum tracking fidelity (middle) and vigour (right) displayed by animals in the two conditions. **n**, Average turning response during courtship in trials where courtship was induced by activation of P1 neurons (left) or spontaneously initiated (right). **o**, Fraction of males actively engaged in courtship (TI > 0.3) over the course of a 10-min trial in P1-induced trials (left) and spontaneously initiated trials (right). Dashed lines indicate LED onset (red) or the onset of visual motion (right). All shaded line plots are mean ± s.e.m.; $^{*}P < 0.05$; n.s., $P > 0.05$; details of statistical analyses and sample sizes are given in Supplementary Table 1.

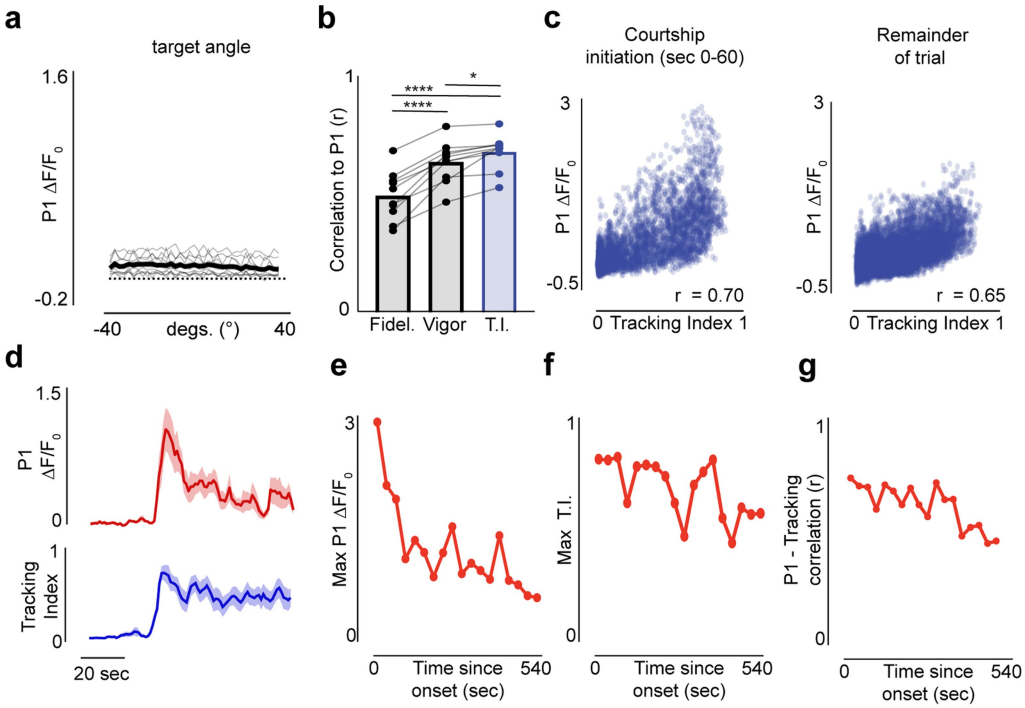

Extended Data Fig. 5 | P1 neurons are dynamic but strongly correlated to the intensity of courtship pursuit. a, The average activity of P1 neurons ($\Delta F/F_0$) plotted against the position of the 'female' visual target. Thin grey lines are individual animals, black line is the average across animals. **b**, Correlation between P1 activity ($\Delta F/F_0$) and the tracking fidelity, tracking vigour, and tracking index (T.I.) of males. Individual data points are individual animals. **c**, P1 activity ($\Delta F/F_0$) plotted against tracking index at the onset of courtship (first 60 s; left) and for the remainder of the trial (right). **d**, Top, average response of P1 neurons aligned to the onset of courtship. Bottom, average tracking index aligned to the onset of courtship. Note that P1 activity is disproportionally elevated in the first few seconds, indicating that it may reflect additional aspects of the male's internal state or behaviour that we are not measuring. **e**, Maximum P1 activity observed across animals as a function of time since courtship initiation. **f**, Maximum tracking index observed across animals as a function of time since courtship initiation. **g**, Average correlation between P1 activity ($\Delta F/F_0$) and the tracking index across animals as a function of time since courtship initiation. All shaded line plots are mean ± s.e.m.; $^{****}P < 0.0001$, $^{*}P < 0.05$; details of statistical analyses and sample sizes are given in Supplementary Table 1.

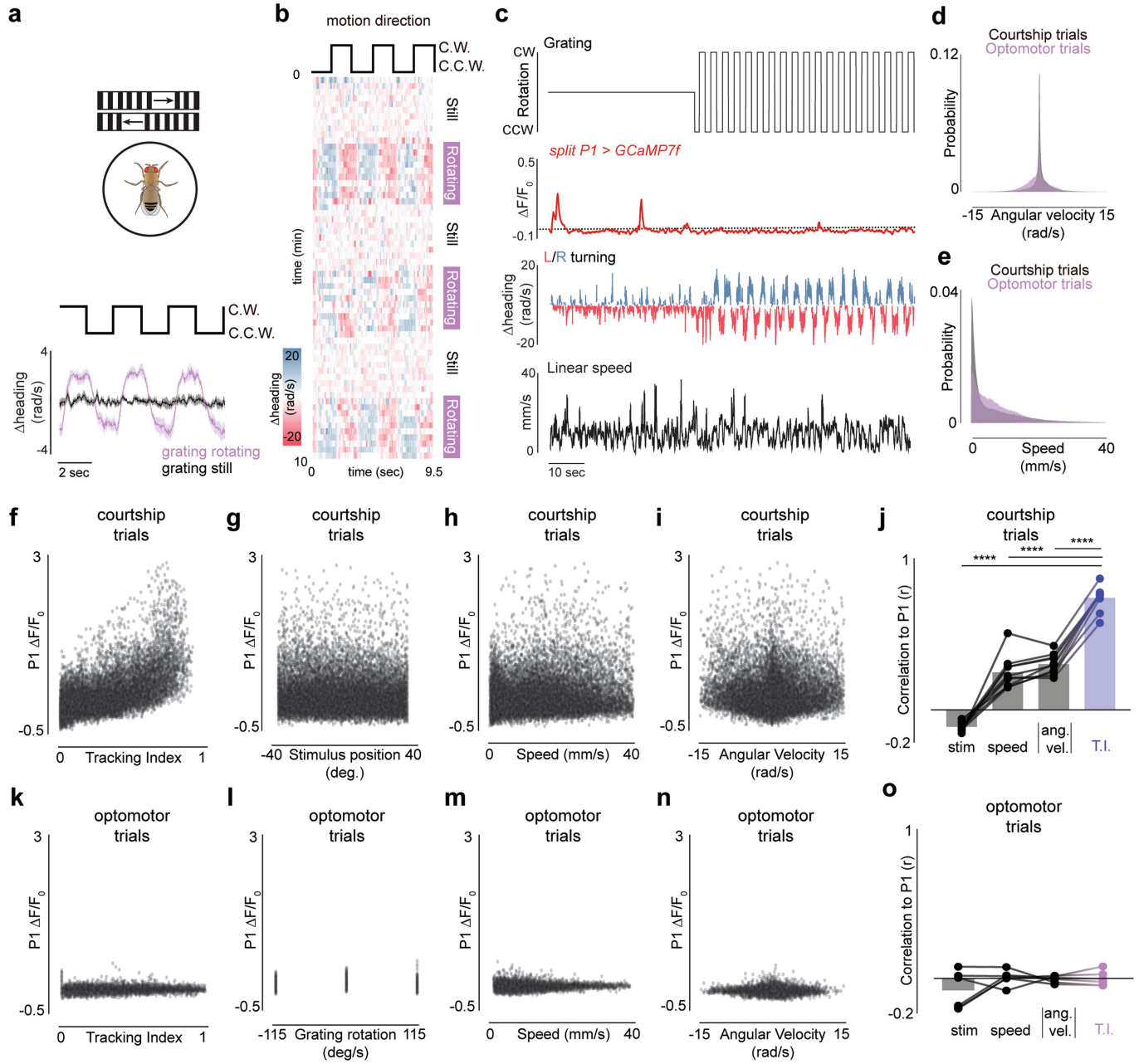

Extended Data Fig. 6 | P1 neuron activity is uncorrelated with the motor implementation of courtship. a, Schematic of preparation for evoking optomotor responses using wide-field motion (top), and the turning responses of animals presented with alternating-direction wide-field motion. **b**, Example of a male's turning during an optomotor trial. Each row consists of three stimulus cycles. Purple bars indicate when the grating is rotating. **c**, Example of the functional response ($\Delta F/F_0$) of P1 neurons during an optomotor trial, before and during periods when the grating turned, as well as the angular velocity and linear speed of the animal. **d**, Histogram of angular velocities observed during courtship trials (grey) and during optomotor trials (purple). **e**, Histogram of linear speeds observed during courtship trials (grey) and during optomotor trials (purple). **f**–**i**, Scatter plots of P1 activity against the tracking index (**f**), stimulus position (**g**), linear speed (**h**) and angular velocity (**i**) of all animals during courtship trials. **j**, Correlation between P1 activity and the parameters explored in **f**–**i** during courtship trials. Individual data points are animals. **k**–**n**, Scatter plots of P1 activity against the optomotor tracking index (**k**), velocity of the grating (**l**), linear speed (**m**) and angular velocity (**n**) of all animals during optomotor trials. **o**, Correlation between P1 activity and the parameters explored in **k**–**n** during optomotor trials. Individual data points are animals. All shaded line plots are mean ± s.e.m.; $^{*}P < 0.05$, $^{**}P < 0.01$, $^{***}P < 0.001$, $^{****}P < 0.0001$. Details of statistical analyses and group sizes are given in Supplementary Table 1.

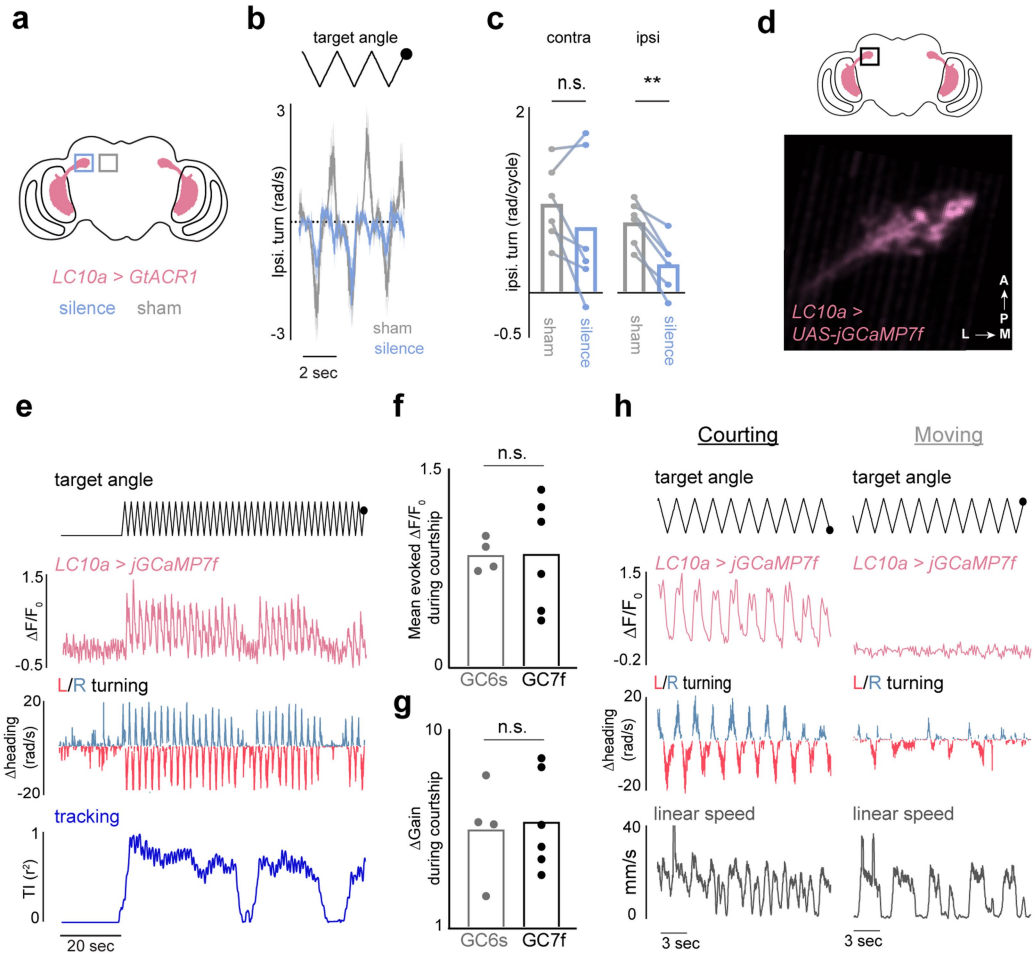

Extended Data Fig. 7 | LC10a signalling is necessary and amplified during courtship. a, Schematic of LC10a neurons expressing GtACR1 with approximate ROIs used for silencing (or sham-silencing) in a single hemisphere. **b**, Average turning of one male to the visual stimulus during silencing of LC10a neurons in the right hemisphere versus sham trials. Note that male fails to execute turns in the direction ipsilateral to silencing. **c**, Average turning in the directions ipsilateral and contralateral to the hemisphere where LC10a was silenced, compared to sham trials. **d**, Image of LC10a axon terminals expressing jGCaMP7f in the AOTu. **e**, Example of functional response ($\Delta F/F_0$) of LC10a neurons expressing jGCaMP7f during a courtship. Note that, in contrast to recordings made using GCaMP6s (Fig. 2b), calcium transients return to baseline in between responses with this faster indicator. **f**, Average evoked LC10a responses ($\Delta F/F_0$) to one stimulus cycle for animals expressing GCaMP6s versus jGCaMP7f. **g**, Average change in LC10a gain (distance between peak and trough of evoked responses) for animals expressing GCaMP6s versus jGCaMP7f. **h**, Example of LC10a functional responses during courtship versus during a later period of undirected running with similar linear speed. All shaded line plots are mean ± s.e.m.; n.s., $P > 0.05$; $^{**}P < 0.01$. Details of statistical analyses and group sizes are given in Supplementary Table 1.

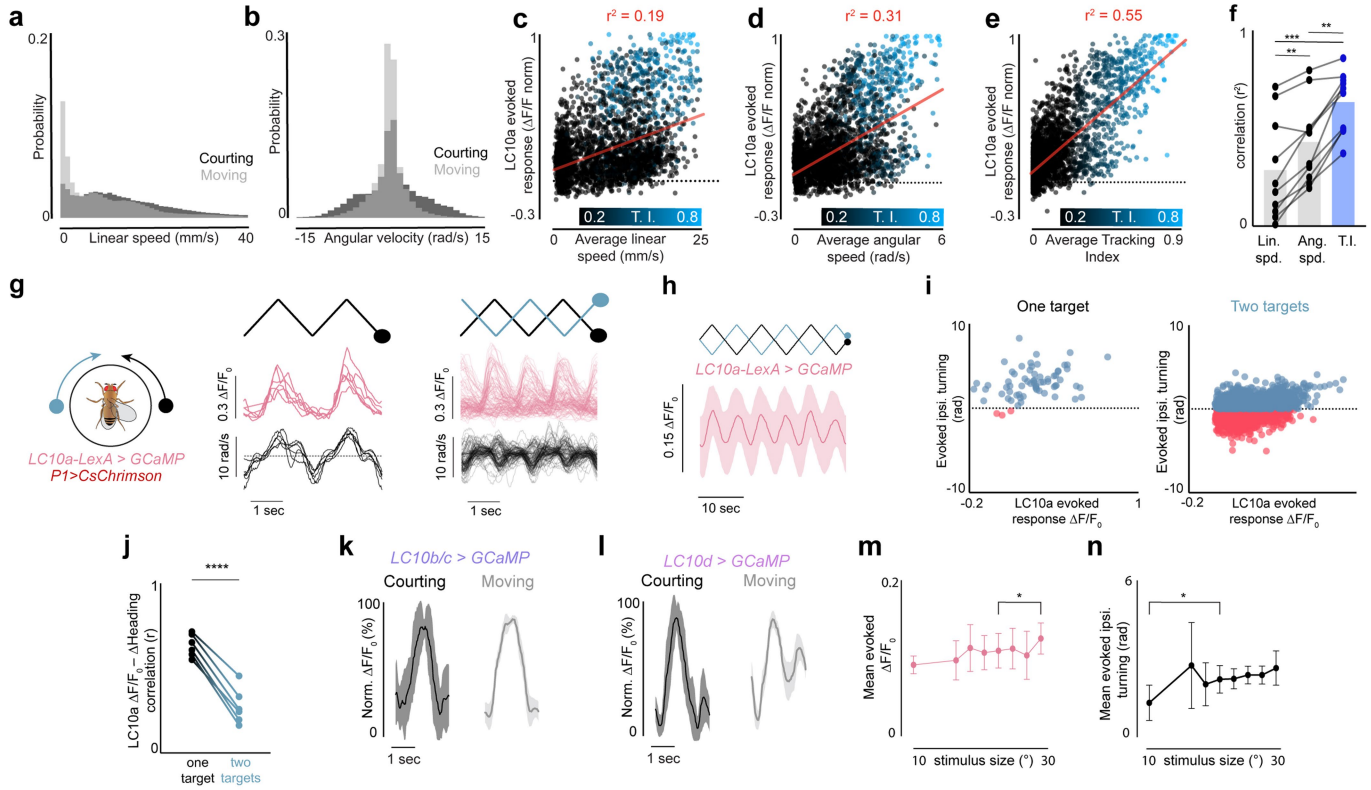

Extended Data Fig. 8 | LC10a gain can be dissociated from the motor implementation of courtship pursuit. a, **b**, Histograms of the linear speeds (**a**) and angular velocities (**b**) exhibited by animals in periods classified as courtship versus periods classified as 'moving'. **c**, Average evoked LC10a activity ($\Delta F/F_0$) when the stimulus swept across the ipsilateral hemifield versus the average linear speed of animals in the same time period, colour coded by the average tracking index during the sweep. Red line is the linear fit. **d**, **e**, As in **c** but plotted against the average angular speed (**d**) or average tracking index (**e**) exhibited by animals. **f**, Correlations between LC10a activity and the linear speed, angular speed, and tracking index exhibited by animals. Individual data points denote individual animals. **g**, Left, schematic of animal being presented with two identical 'female' targets, moving in opposition and thus yielding identical stimulation to both eyes. Middle, example of LC10a functional responses plotted against the position of a single target (top) and animal turning responses (bottom). Right: as for middle, but later in the trial when the animal was presented with two opposing targets. P1 neurons were activated continuously. Note that LC10a neurons responded even when the male failed to turn ipsilaterally when two targets were present. **h**, Average LC10a activity during presentation of two opposing visual targets (top). **i**, Left, average evoked LC10a activity during ipsilateral sweeps of the visual target versus the total turning exhibited in the direction of the visual target during the same period. Right, average evoked LC10a activity during ipsilateral sweeps of either of the two visual targets versus the total turning exhibited in the direction of the visual target during the same period. **j**, Correlation between LC10a evoked responses and ipsilateral turning. Individual data points denote individual animals. **k**, Average peak-normalized responses ($\Delta F/F_0$) of LC10b/c neurons during courtship versus during locomotion. **l**, As in **k** but for LC10d neurons. **m**, **n**, Average evoked LC10a functional response ($\Delta F/F_0$, **k**) and average evoked ipsiversive turning (**n**) as a function of the average angular size of the visual target on each stimulus cycle. All shaded line plots are mean ± s.e.m.; n.s., $P > 0.05$; $^*P < 0.05$, $^{**}P < 0.01$, $^{***}P < 0.001$. Details of statistical analyses and group sizes are given in Supplementary Table 1.

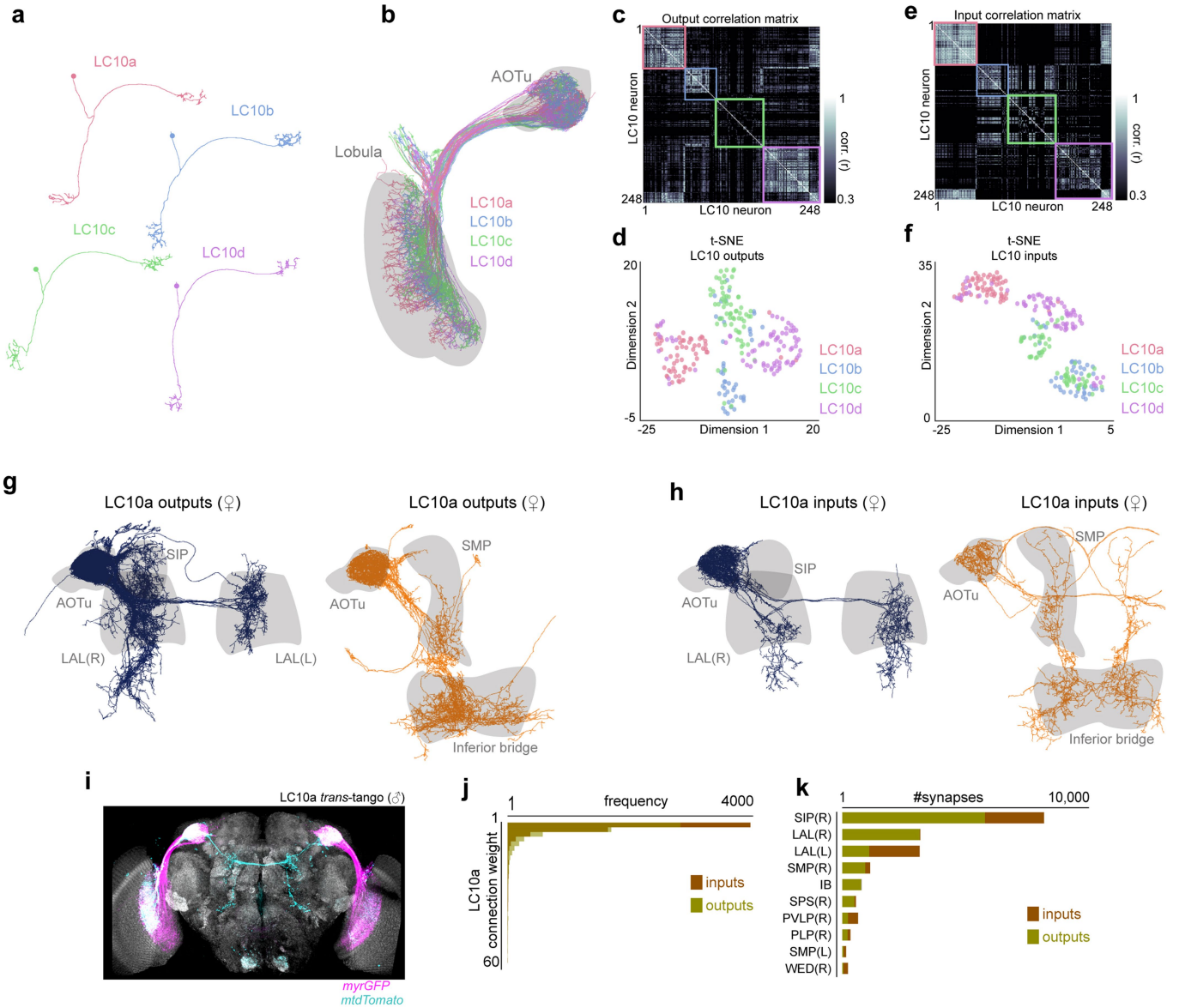

Extended Data Fig. 9 | LC10a neurons exhibit sparse and selective connectivity in the central brain. a, Examples of identified LC10a, LC10b, LC10c, and LC10d neurons in the female hemi-brain connectome[23]. **b**, Morphology of all identified LC10a-d neurons ($n = 248$). **c**, Correlation matrix of the outputs from all LC10 neurons, sorted by their assigned subtype. Note that individual subtypes have strongly correlated outputs that are largely distinct from the output patterns of other subtypes. **d**, *t*-SNE plot of the output connectivity matrix of all identified LC10 neurons, labelled according to the manually assigned subtype. The output connectivity naturally segregates LC10 neurons into four groups. **e**, **f**, Same as **c**, **d** but based on the input connections to LC10 neurons in the AOTu. **g**, Morphology of all non-visual output neurons from LC10a neurons with at least 10 synaptic connections, grouped by projections to the LALs (left) versus to the inferior bridge (IB; right). **h**, As in **g** but for non-visual input neurons to LC10a neurons in the AOTu. **i**, Representative example of trans-synaptic tracing of LC10a neurons in the male using trans-Tango[24]. Magenta denotes labelled LC10a neurons, and cyan the labelled postsynaptic partners. Similar results were obtained across four male brains. **j**, Histogram of synaptic weights between all LC10a neurons and their postsynaptic partners. **k**, Number of input and output synapses to and from LC10a neurons from the 10 most common brain regions (superior intermediate protocerebrum (SIP), lateral accessory lobe (LAL), superior medial protocerebrum (SMP), inferior bridge (IB), superior posterior slope (SPS), posterior ventrolateral protocerebrum (PVLP), posteriolateral protocerebrum (PLP), superior medial protocerebrum (SMP), wedge (WED)). R and L indicate the right and left hemisphere, respectively.

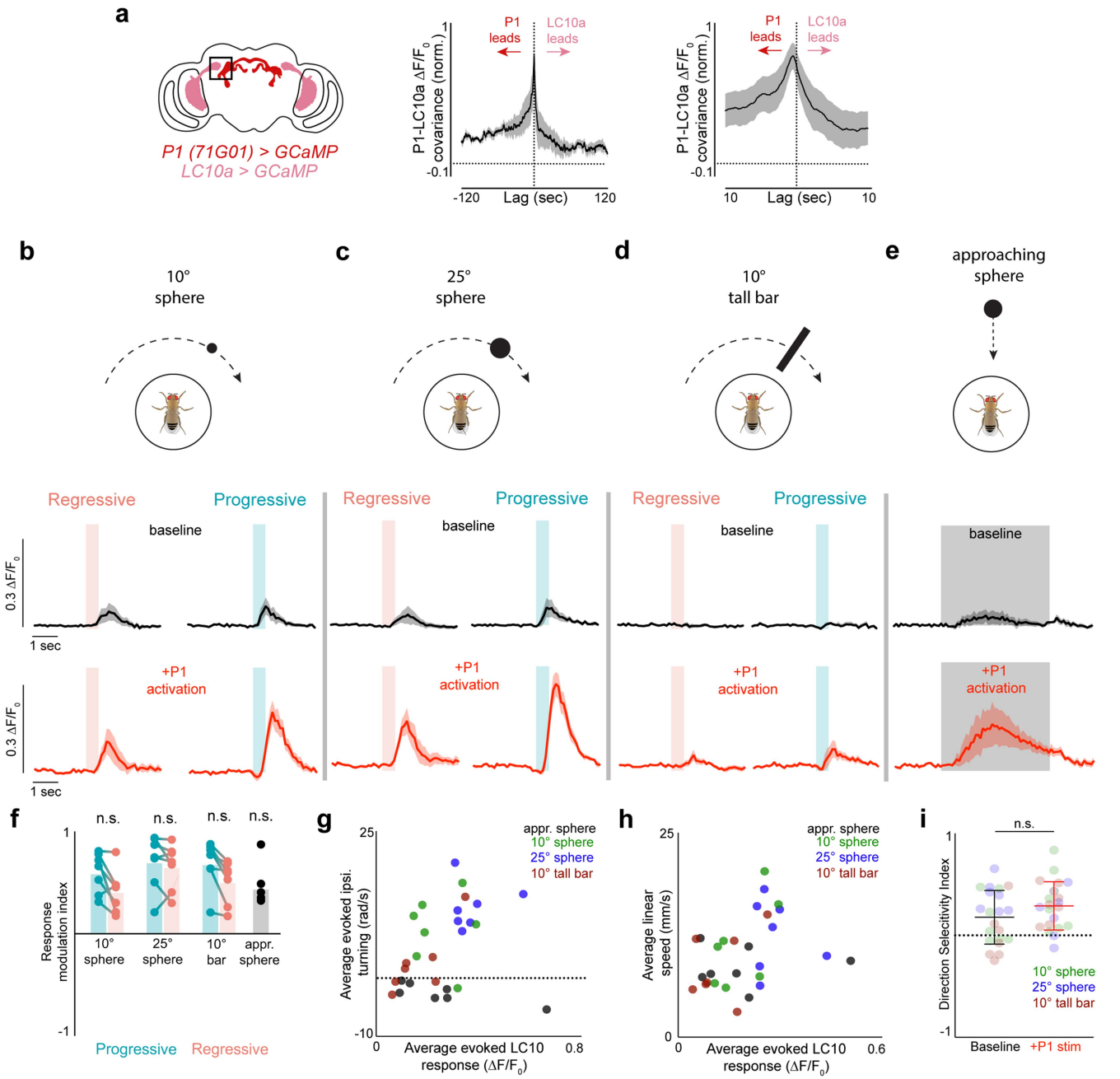

Extended Data Fig. 10 | P1 neurons enhance the gain of LC10a neurons. **a**, Left, schematic of synchronous recordings from P1 neurons in the LPC and LC10a neurons in the AOTu. Middle, cross-covariance of P1 neuron activity and LC10a activity during spontaneous courtship trial. Right, as for middle, but zoomed in to highlight that P1 neuron activity leads LC10a activity. Maximum covariance occurred at lag of −500 ms. **b**, LC10a responses to presentation of a 10° sweeping dot in the progressive or regressive direction before and during activation of P1 neurons. Top, average LC10a response during presentation of a regressively (orange) or progressively (blue) moving stimulus in the absence of P1 activation. Bottom, average LC10a response during presentation of a regressively (orange) or progressively (blue) moving stimulus in the presence of P1 activation. **c**–**e**, As in **b** but for a sweeping 25° sphere (**c**), a sweeping 10° wide tall bar (**d**), or an approaching sphere expanding from 10° at 20°/s (**e**). Red indicates P1stimulation and black indicates pre-stimulation baseline throughout. **f**, Response modulation index (see Methods) for each stimulus presented before and during P1 activation, indicating that responses to the distinct visual stimuli are near-uniformly enhanced. **g**, Average evoked ipsilateral turning in response to progressive motion of the different targets during P1 activation, plotted against the average evoked LC10a response in the same period. Note that turning responses evoked by the motion of these diverse stimuli were proportional to the magnitude of LC10a evoked calcium transients: sweeping dots evoked the strongest turns, bars evoked much weaker turns, and slowly looming spheres did not elicit any turning on average, presumably because both eyes were stimulated equally. **h**, Average evoked linear speed in response to progressive motion of the different targets during P1 activation, plotted against the average evoked LC10a response in the same period. **i**, Direction selectivity index (see Methods) for sweeping stimuli presented during baseline recordings or during continuous P1 activation. Positive values indicate a preference for progressive motion, negative values indicate preference for regressive motion. All shaded line plots are mean ± s.e.m.; n.s., $P > 0.05$. Details of statistical analyses and sample sizes are given in Supplementary Table 1.

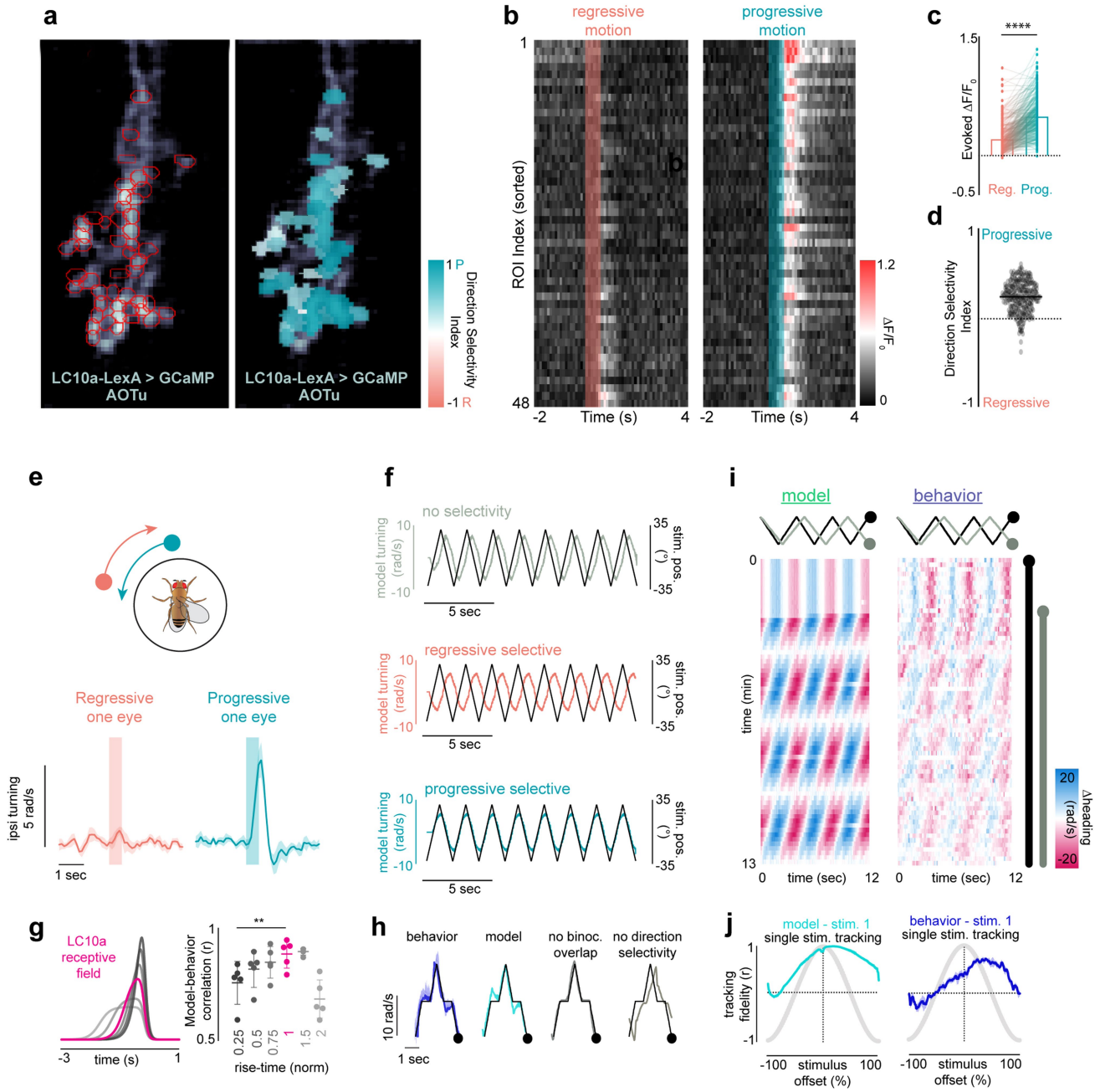

Extended Data Fig. 11 | Motion-direction selectivity during courtship pursuit. a, Left, example image of LC10a–LexA axon terminals in the AOTu, with 48 ROIs of strongly correlated pixels automatically selected using the CaImAn-CNMF framework[48] overlayed. Right, as for left, but with ROIs colour-coded according to their exhibited direction selectivity index (positive values indicate a preference for progressive motion, negative values indicate preference for regressive motion). **b**, Heat map of the average evoked responses to progressive (right) and regressive (left) sweeps of the 25° sphere during P1 activation for the 48 ROIs shown in **a**. Each row represents the average evoked fluorescence across 10 trials for each ROI. **c**, Average evoked responses to a progressively versus regressively moving 25° dot across all ROIs from all animals (300 ROIs across 7 males). **d**, Direction selectivity index for all ROIs across animals (see Methods). Black line denotes zero; positive values indicate a selectivity for progressive motion, negative values indicate a selectivity for regressive motion. **e**, Top, schematic of monocular stimulation. 'Female' targets were presented to one eye alone, and moved in either the regressive or progressive direction with respect to that eye with a 5-s ISI. Bottom, average turning of males in response to monocular stimuli moving regressively (left) or progressively (right). **f**, Turning responses of LC10a circuit model without motion-direction selectivity, with regressive-motion selectivity, and with progressive-motion selectivity. **g**, Left, normalized LC10a receptive fields with varying rise-times (κ, see Methods). Right, correlation between predicted and actual responses to the simple stimulus in **f** for the receptive fields shown to the left. **h**, From left: average turning response to a single stimulus cycle; predicted response from full model to a single stimulus cycle; predicted response of a model with no binocular overlap; predicted response of a model not selective for progressive versus regressive motion. **i**, Example of predicted versus actual turning response to two targets with a drifting phase-offset (as in Fig. 4d) across the courtship trial. Black line indicates when first target is present, grey line indicates when the second target is present. **j**, Left, average correlation between stimulus 1 and predicted turning (cyan) during dual dot presentations. Right, average correlation between stimulus 1 and the turning of males during dual dot presentations. In grey is what the correlation to stimulus 1 would be if the animal perfectly tracked stimulus 2. Positive x-values indicate that the first stimulus leads in phase. All shaded line plots are mean ± s.e.m.; $^{**}P < 0.01$, $^{****}P < 0.0001$. Details of statistical analyses and sample sizes are given in Supplementary Table 1.

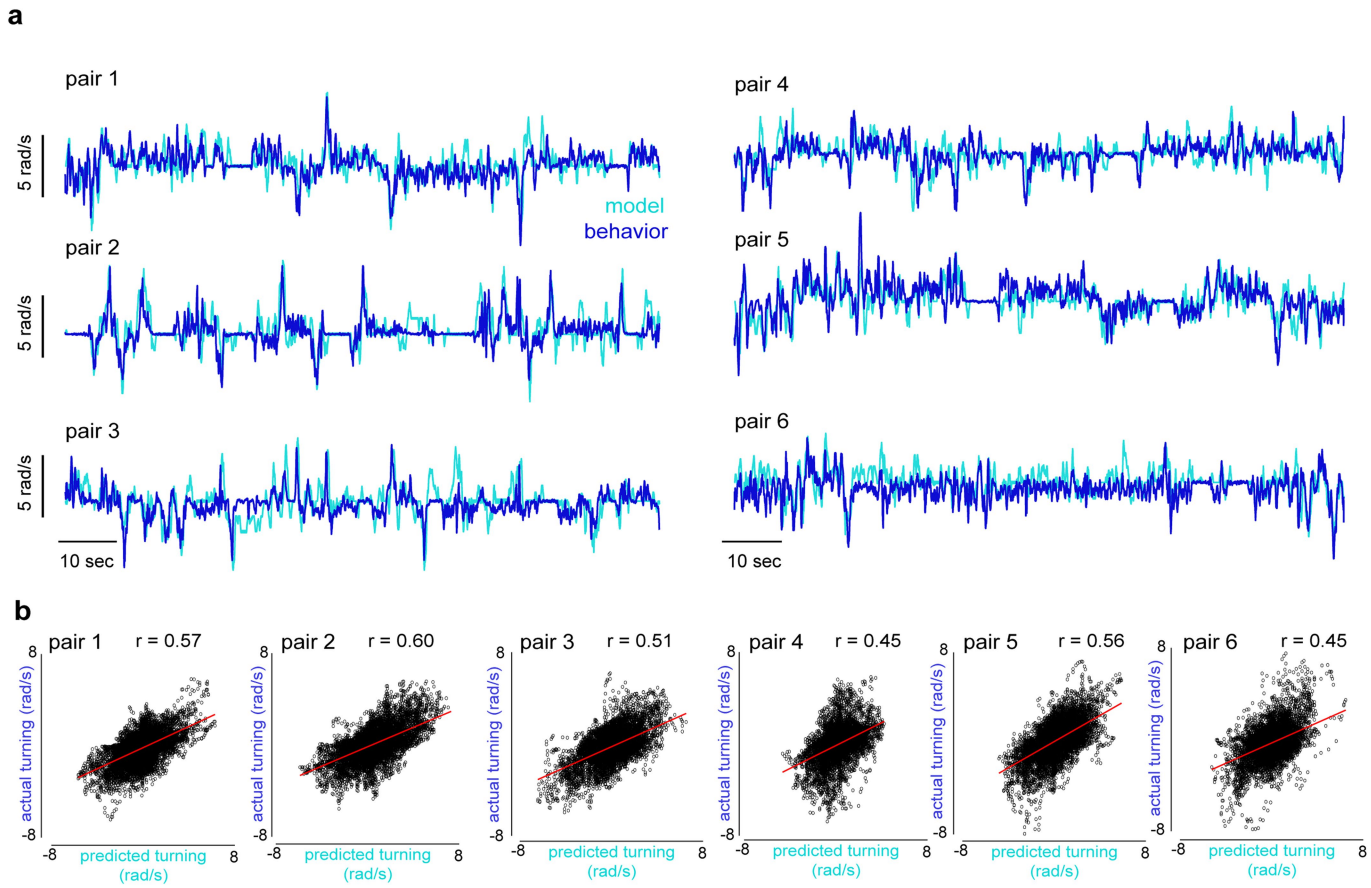

Extended Data Fig. 12 | Network model predicts turning dynamics of freely courting males. a, Examples of predicted versus actual turning of freely courting males over the first 100 s of courtship. **b**, Frame-by-frame predicted versus actual male turning over the course of the full courtship trials for the pairs shown in **a** (5–10 min); red line shows the linear fit. Details of statistical analyses and sample sizes are given in Supplementary Table 1.

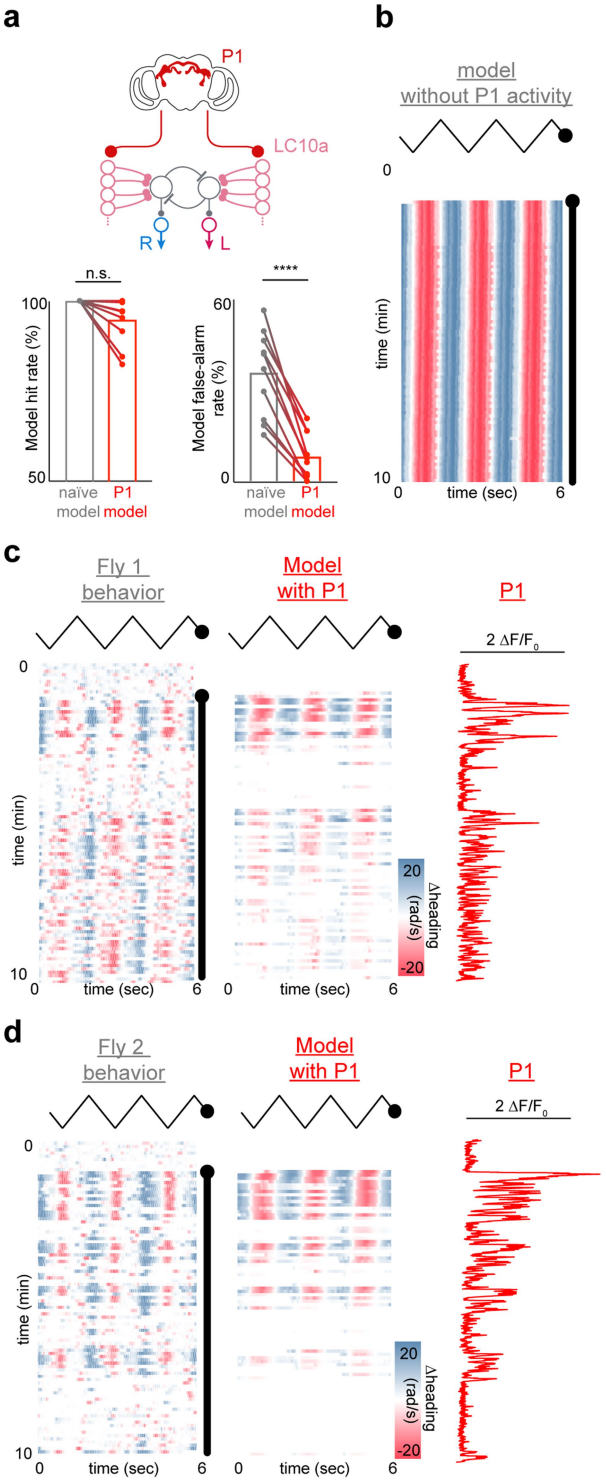

Extended Data Fig. 13 | Incorporating P1 neural activity improves model performance. a, Hit rate (fraction of predicted turns accompanied by a real turn; true positive rate) and false-alarm rate (fraction of predicted turns not accompanied by a real turn; false positive rate) of the naive model (lacking P1 input) versus when input current to LC10a neurons is scaled by the functional responses of P1 neurons. **b**, Example of the predicted turning over a courtship trial by a model lacking P1 input (as in Fig. 4a) in which input current to LC10a neurons is consistently high. **c**, **d**, Two examples of actual (left) versus predicted (middle) turning responses when the activity of P1 neurons (right) is incorporated into the model. Compare to model without P1 input in **b**. Black lines indicate when stimulus is oscillating. Details of statistical analyses and sample sizes are given in Supplementary Table 1.

nature research

Corresponding author(s): Vanessa Ruta

Last updated by author(s): Sep 4, 2020

Reporting Summary

Nature Research wishes to improve the reproducibility of the work that we publish. This form provides structure for consistency and transparency in reporting. For further information on Nature Research policies, see our Editorial Policies and the Editorial Policy Checklist.

Statistics

For all statistical analyses, confirm that the following items are present in the figure legend, table legend, main text, or Methods section.

n/a	Confirmed
☐	☒ The exact sample size (*n*) for each experimental group/condition, given as a discrete number and unit of measurement
☐	☒ A statement on whether measurements were taken from distinct samples or whether the same sample was measured repeatedly
☐	☒ The statistical test(s) used AND whether they are one- or two-sided *Only common tests should be described solely by name; describe more complex techniques in the Methods section.*
☐	☒ A description of all covariates tested
☐	☒ A description of any assumptions or corrections, such as tests of normality and adjustment for multiple comparisons
☐	☒ A full description of the statistical parameters including central tendency (e.g. means) or other basic estimates (e.g. regression coefficient) AND variation (e.g. standard deviation) or associated estimates of uncertainty (e.g. confidence intervals)
☐	☒ For null hypothesis testing, the test statistic (e.g. *F*, *t*, *r*) with confidence intervals, effect sizes, degrees of freedom and *P* value noted *Give P values as exact values whenever suitable.*
☒	☐ For Bayesian analysis, information on the choice of priors and Markov chain Monte Carlo settings
☒	☐ For hierarchical and complex designs, identification of the appropriate level for tests and full reporting of outcomes
☐	☒ Estimates of effect sizes (e.g. Cohen's *d*, Pearson's *r*), indicating how they were calculated

Our web collection on statistics for biologists contains articles on many of the points above.

Software and code

Policy information about availability of computer code

Data collection	Animal trajectories on the spherical treadmill were monitored by the FicTrac2.0 software. Visual stimuli were generated in the ViRMEn (2016-02-12 release) virtual reality environment using custom scripts, run via MATLAB R2014b (MathWorks). All modeling was done in MATLAB 2019a using custom functions. Two-photon calcium imaging was performed using Praire View 5.4 (Bruker Corporation). Fluorescence time-series were extracted using FIJI (v. 2.0.0-rc-69/1.52p,ImageJ, NIH). Motion correction was done using NoRMCorre (Flatiron Institute). Semi-supervised ROI extraction for individual axonal boutons was done using CaImAn (Flatiron Institute). Animals were monitored using the FlyCapture2 Software Development Kit (FLIR) during behavioral assays.
Data analysis	We used MATLAB R2019a for analysis, and a mixture of MATLAB R2019a and GraphPad Prism 9 for statistics and data visualization. Custom MATLAB code was written for a theoretical model. Circular statistics were computed using the Circular Statistics Toolbox (1.21.0.0; Berens, 2009)

For manuscripts utilizing custom algorithms or software that are central to the research but not yet described in published literature, software must be made available to editors and reviewers. We strongly encourage code deposition in a community repository (e.g. GitHub). See the Nature Research guidelines for submitting code & software for further information.

Data

Policy information about availability of data

All manuscripts must include a data availability statement. This statement should provide the following information, where applicable:

- Accession codes, unique identifiers, or web links for publicly available datasets
- A list of figures that have associated raw data
- A description of any restrictions on data availability

All data underlying figures are available as supplemental materials. Raw data is available upon request from the corresponding author. Code underlying the model is available at XXXX

Field-specific reporting

Please select the one below that is the best fit for your research. If you are not sure, read the appropriate sections before making your selection.

☒ Life sciences ☐ Behavioural & social sciences ☐ Ecological, evolutionary & environmental sciences

For a reference copy of the document with all sections, see nature.com/documents/nr-reporting-summary-flat.pdf

Life sciences study design

All studies must disclose on these points even when the disclosure is negative.

Sample size	Sample sizes were not predetermined, but deemed appropriate based on the large effect size and consistency across animals. Our sample sizes are in alignment with other recent papers with similar tethered imaging preparations (e.g. Kohatsu & Yamamoto (2015); Ribeiro et al. (2018); Seeholzer et al. (2018)).
Data exclusions	For tethered courtship assays, unless otherwise noted, only experiments during which animals exhibited courtship towards the visual targets were included for analysis, selected based on a tracking index > 0.3 for at least 1 second and the presence of at least one unilateral wing extension. For modeling of free behavior, only flies that courted for >90% of the time before copulation were included. For wide-field motion experiments, only flies that exhibited an average optomotor response of at least 5rad/s were included. Beyond these criteria, data was only excluded in the event of an acquisition error or data corruption (e.g. dropped frames or failed image stitching).
Replication	All attempts at replication were successful. All experiments were replicated at least across multiple days with independent biological replicates and often across multiple months. All experiments were replicated across at minimum 3 animals.
Randomization	This is not relevant to the study as behavior and activity patterns were quantitative assessments with no "treatment" groups. Controls were done within animals (e.g. each animal received both periods of "sham" optogenetics and targeted optogenetic silencing), and animals were thus not randomized.
Blinding	Blinding was not relevant for this study as behavior was assessed quantitatively based on objective, measured criteria.

Reporting for specific materials, systems and methods

We require information from authors about some types of materials, experimental systems and methods used in many studies. Here, indicate whether each material, system or method listed is relevant to your study. If you are not sure if a list item applies to your research, read the appropriate section before selecting a response.

Materials & experimental systems

n/a	Involved in the study
☐	☒ Antibodies
☒	☐ Eukaryotic cell lines
☒	☐ Palaeontology and archaeology
☐	☒ Animals and other organisms
☒	☐ Human research participants
☒	☐ Clinical data
☒	☐ Dual use research of concern

Methods

n/a	Involved in the study
☒	☐ ChIP-seq
☒	☐ Flow cytometry
☒	☐ MRI-based neuroimaging

Antibodies

Antibodies used	Primary antibodies used were mouse anti-Brp (nc-82, Developmental Studies Hybridoma bank), rabbit anti-GFP (A11122, Invitrogen), and rat anti-HA (11867423001, Roche). Secondary antibodies used were AF555 goat anti-Rat (A21434, Invitrogen), AF633 goat anti-mouse (A21052, Invitrogen), and AF488 goat anti-rabbit (A11034, Invitrogen).

Validation	All antibodies used in this study are commercial and previously validated for immunohistochemistry in Drosophila, as described on the manufacturers' website. Primary antibodies have also been validated for application in Drosophila by the FlyLight project at Janelia Research Campus (https://www.janelia.org/project-team/flylight/protocols.).

Animals and other organisms

Policy information about studies involving animals; ARRIVE guidelines recommended for reporting animal research

Laboratory animals	All flies used for behavioral analysis were between 2-7 days old. Flies used for free behavior were 3-5 day old virgins, one male and one female per pair. Flies used for tethered behavior and functional experiments were all 2-3 day-old males (with the exception of 9 females tested for spontaneous courtship). Flies used for immunohistochemistry were 30-40 days old. Images of brains are all males. Please refer to the methods and Supplemental Table 1 for further description of research animals
Wild animals	No wild animals were used in this study.
Field-collected samples	No field-collected animals were used in this study.
Ethics oversight	No ethical approval was required because all experiments in this study were performed on Drosophila melanogaster.

Note that full information on the approval of the study protocol must also be provided in the manuscript.